COMPLEX FILTERS AS CASCADE OF BUFFERED GINGELL STRUCTURES: DESIGN FROM BAND-PASS CONSTRAINTS

A Thesis
presented to
the Faculty of California Polytechnic State University,
San Luis Obispo

In Partial Fulfillment
of the Requirements for the Degree
Master of Science in Electrical Engineering

by
Nicole Marie Hay
June 2017

COMMITTEE MEMBERSHIP

TITLE:	Complex Filters as Cascade of Buffered Gingell Structures: Design from Band-Pass Constraints
AUTHOR:	Nicole Marie Hay
DATE SUBMITTED:	June 2017
COMMITTEE CHAIR:	Vladimir Prodanov, Ph.D. Associate Professor of Electrical Engineering
COMMITTEE MEMBER:	David Braun, Ph.D. Professor of Electrical Engineering
COMMITTEE MEMBER:	Wayne Pilkington, Ph.D. Associate Professor of Electrical Engineering

ABSTRACT

Complex Filters as Cascade of Buffered Gingell Structures: Design from Band-Pass Constraints

Nicole Marie Hay

Complex filters are multi-input, multi-output networks designed to discriminate based upon the relative phase difference between input signals. Complex filters find application in modern wireless systems for single sideband transmission and image-reject reception. This thesis presents one active complex filter implementation using two operational amplifiers per stage, termed "type-II" topology. The "type-II" originates from the passive RC-CR polyphase topology presented by Gingell in his 1973 paper, "Single sideband modulation using sequence asymmetric polyphase networks." This new topology gains several advantages over existing complex filter implementations, namely "cascadability" (multiple sections placed in series to create a higher-order response) without altering the characteristics of each individual stage. In addition to describing the derivation of the topology and its performance relative to existing topologies, this thesis investigates the passband characteristics of a general higher-order filter and provides a passband-centric design approach through derivations of closed form expressions for passband gain and bandwidth. The thesis includes a five-stage design example using this approach in addition to an implementation, its characterization, and its comparison to the derived expressions and simulations.

Keywords: Complex filter, positive frequency, negative frequency, quadrature, cascade

TABLE OF CONTENTS

Page

LIST OF TABLES

Table Page

LIST OF FIGURES

Figure Page

1. INTRODUCTION

1.1 Purpose of Study

Complex filters consist of two-input, two-output networks designed to accept a pair of quadrature signals and discriminate based on the relative phase between those two signals. They find use in modern wireless systems for single sideband transmission or for image-reject reception [1-6]. Both passive and active implementations exist; in the category of active implementations, op-amps [2] or operational transconductance amplifiers [3] are the most common active components. The passive Gingell topology, extensively studied for its properties and low sensitivity to component variation, stands out as one of the most well-known structures [5] [6].

This thesis introduces one possible implementation of a two op-amp "buffered Gingell" type structure and discusses the design methodology of higher-order filters based on bandpass constraints. Use of minimal active components for buffering purposes in a multi-stage Gingell networks presents the opportunity to develop unique design strategies and examine the difficulties of implementing over-constraint designs.

The following provides an overview of the concept of positive and negative frequencies, differential and complex networks, and a well-known existing implementation of a complex filter. This leads to the introduction of a new topology, termed "type-II", which requires the fewest number of active components. This topology shares similarities in design with another topology, called "type-I", discussed by Johnston in, "Complex filters as a cascade of buffered Gingell

structures: design from stop-band constraints" [7]. Because of the broad topic of complex filters and extensive characterization of the new topologies, the study resulted in two theses. "Complex filters as a cascade of buffered Gingell structures: design from stop-band constraints" focuses on the type-I topology, investigation of stop-band characteristics, and Monte Carlo Analysis. This thesis report focuses on the type-II topology, investigation of passband characteristics, and a passband-centric design approach. This includes examination of the type-II topology for mathematical confirmation, implementation results, and general design guidelines and issues. The analysis makes use of a mathematical modeling tool and circuit simulation program in addition to mathematical derivations and necessary approximations to explain the topology derivation and performance.

1.2 Positive and Negative Frequency

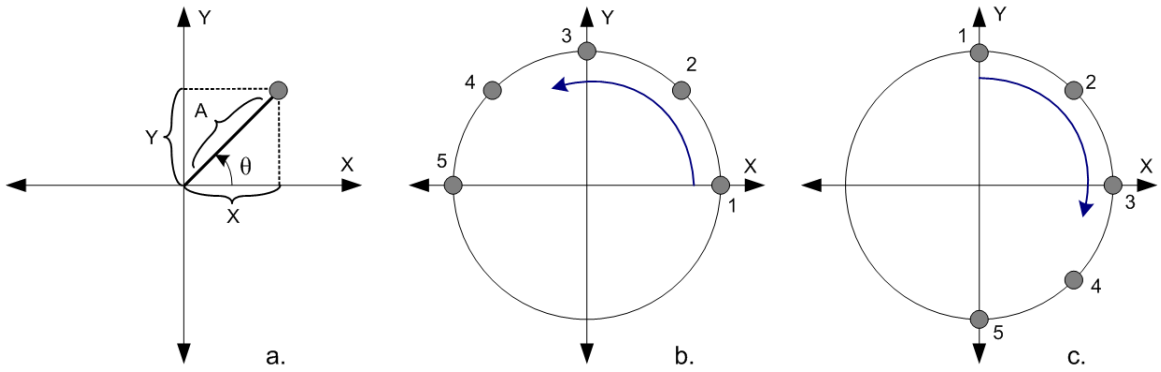

Figure 1. Component definition and rotation direction definition, a. X and Y components of a rotating vector, b. Counterclockwise (positive) rotation, c. Clockwise (negative) rotation

The components of a rotating vector expressed in complex number notation, i.e. $x(t) + jy(t)$, can also be expressed as complex exponentials, $Ae^{j\theta(t)}$ (Figure 1a). Complex number notation corresponds to the Cartesian coordinate system, while complex exponential notation corresponds to the polar coordinate convention. A

vector with fixed magnitude and counterclockwise direction of rotation (Figure 1b) expressed as a complex exponential:

$$\frac{A}{\sqrt{2}} cos\ \omega t + j \frac{A}{\sqrt{2}} sin\ \omega t = Ae^{j\omega t} \quad (1)$$

Based on the sign of the end complex exponential exponent, we define this vector's direction of rotation as "positive". Similarly, a clockwise rotating vector (Figure 1c) expressed mathematically:

$$\frac{A}{\sqrt{2}} cos\ \omega t - j \frac{A}{\sqrt{2}} sin\ \omega t = Ae^{-j\omega t} \quad (2)$$

Based on the sign of the exponent, we define this rotation as "negative". Interchanging the x and y components in the counterclockwise case (1) results in:

$$\frac{A}{\sqrt{2}} sin\ \omega t + j \frac{A}{\sqrt{2}} cos\ \omega t = \frac{A}{\sqrt{2}} e^{-j\omega t} \quad (3)$$

Observe that expression (3) equates to the clockwise case (2).

To further illustrate that interchanging the x and y components of a rotating vector results in a change in the direction of the vector's rotation, Table 1 and Table 2 provide the position of the vector in the S-plane for both the clockwise and counterclockwise cases.

Table 1. $X = cos\ \theta$, $Y = sin\ \theta$, $X + jY = e^{\phi}$

Position (Fig. 1b)	$\boldsymbol{\theta}$(˚)	$\boldsymbol{\phi}$(˚)
1	0	0
2	45	45
3	90	90
4	135	135
5	180	180

Table 2. X = sin θ, Y = cos θ, X + jY = e^{ϕ}

Position (Fig. 1c)	**θ (°)**	**ϕ(°)**
1	0	90
2	45	45
3	90	0
4	135	-45
5	180	-90

1.3 Differential Circuits (Multi-input Networks)

As mentioned previously, a complex filter is a two-input, two-output network. To better understand its properties, first examine another two-input, two-output network, the differential amplifier. Two characteristics describe a differential amplifier: common-mode characteristics, and differential-mode characteristics. Driving one amplifier input with a small, likely sinusoid, signal and driving the other input with a signal 180° out of phase with the first signal determines differential-mode characteristics (Figure 2, right). Connecting the two inputs to each other and driving them with the same small signal determines common-mode characteristics (Figure 2, left). These two measurements combined represent a performance specification, common mode rejection ratio (CMRR); CMRR measures how well the amplifier rejects common-mode (alike) input signals compared to differential-mode input gain [8].

$$A_{dm} = differential - mode\ voltage\ gain$$
$$A_{cm} = common - mode\ voltage\ gain$$

$$CMRR = \left|\frac{A_{dm}}{A_{cm}}\right|$$

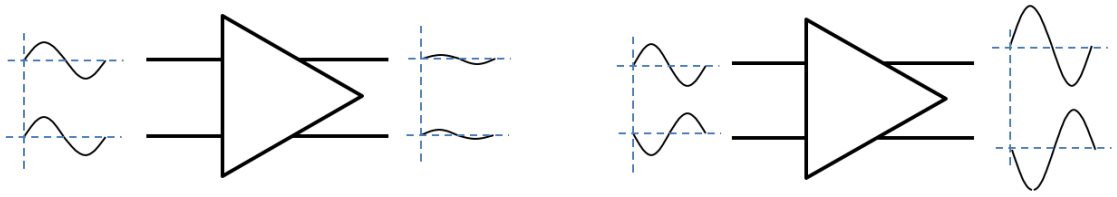

Figure 2. Characterizing a fully differential amplifier, common mode (left), differential mode (right)

In summary, pairs of sinusoids with well-defined phase difference produce the characterizing responses of a differential amplifier. Two sinusoids in phase determine common-mode characteristics. A pair of sinusoids with an 180° phase shift between the two determines the differential-mode characteristics.

1.4 Complex Networks

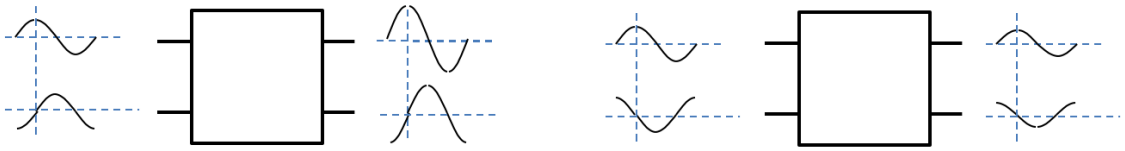

Figure 3. Characterizing complex networks, positive sequence (left), negative sequence (right)

A "complex" network simultaneously receives two input signals and provides two output signals, this pair of signals equates to a vector (or complex) quantity. Complex filters provide two different responses based on the relative phase difference between two applied input signals [9]. These responses are referred to as "positive frequency response" (Figure 3, left) and "negative frequency response" (Figure 3, right). The positive frequency response requires a phase difference between the input signals of 90°:

$$input\ 1 = \frac{A}{\sqrt{2}} cos(\omega t) \Longrightarrow \frac{A}{\sqrt{2}} \quad (4)$$

$$input\ 2 = -\frac{A}{\sqrt{2}} sin(\omega t) \Longrightarrow -j\frac{A}{\sqrt{2}} \quad (5)$$

When considered as a complex quantity, these two responses appear as a counterclockwise rotating vector (1).

The negative frequency response requires a phase difference of negative 90°:

$$input\ 1 = \frac{A}{\sqrt{2}} cos(\omega t) \Longrightarrow \frac{A}{\sqrt{2}} \quad (6)$$

$$input\ 2 = \frac{A}{\sqrt{2}} sin(\omega t) \Longrightarrow j\frac{A}{\sqrt{2}} \quad (7)$$

When considered as a complex quantity, these two responses appear as a clockwise rotating vector (2).

The two responses of a complex filter should, for the purpose of discriminating between positive and negative phase difference inputs, exhibit drastically different responses. One response should pass the signal, analogous to a bandpass filter, while the other response should stop the signal, similar to a notch or bandstop filter.

Complex filters also operate as 90° phase splitters. Because of the asymmetric response for positive versus negative frequency signals, a complex filter produces quadrature signals on the output. Observe that a real sinusoid equates to a combination of a positively rotating vector and a negatively rotating vector:

$$A \cdot cos\ \omega t - j0 = \frac{A}{2} e^{j\omega t} + \frac{A}{2} e^{-j\omega t} \quad (8)$$

This last expression (8) is a form of Euler's identity [10].

The four-input, four-output complex network functions as two complex networks in parallel:

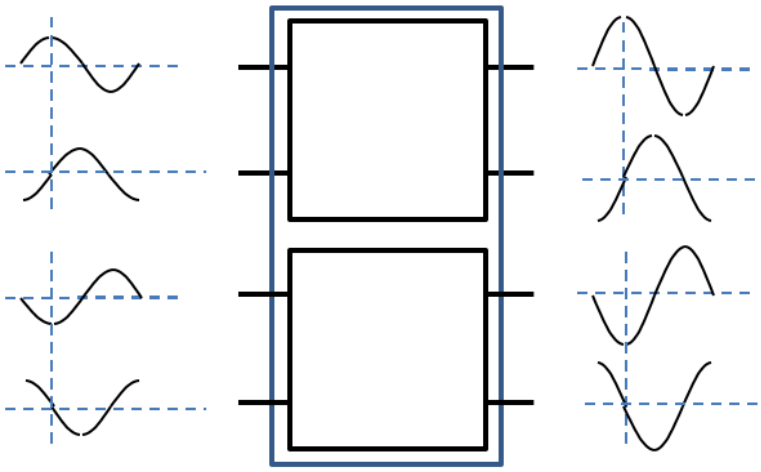

Figure 4. Four-input, four-output complex network, positive sequence response

A four-input, four-output complex network accepts four signals, each 90˚ out of phase with each other. Figure 4 depicts a positive sequence where the first input shifts 90˚ ahead of the second input, the second input shifts 90˚ ahead of the third input, and so on. This complex filter responds to a positive sequence by producing the signals with the same relative phase but larger magnitude on the output. The filter responds to a negative sequence by producing no output signal (not shown). The Gingell network, discussed in the next section, is an example of a four-input, four-output complex network.

1.5 Frequency Behavior of Gingell-type 1st Order Complex Filter

The following discussion introduces the 1st order complex filter response as a partial response of a common 2nd order RLC notch filter (Figure 5) response.

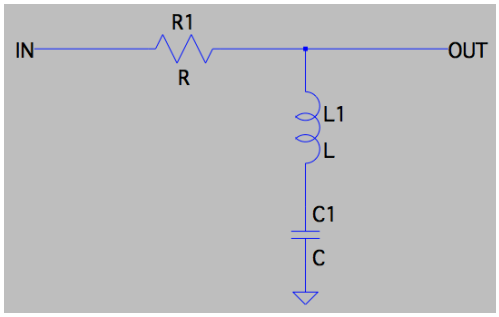

Figure 5. Single stage RLC notch filter

Equations 9-13 derive the transfer function of the circuit in Figure 5:

$$H(s) = \frac{Z_{LC}}{Z_{LC}+R} \quad (9)$$

$$Z_{LC} = sL + \frac{1}{sC} = \frac{s^2CL+1}{sC} \quad (10)$$

$$H(s) = \frac{\frac{s^2CL+1}{sC}}{\frac{s^2CL+1}{sC}+R} \quad (11)$$

$$H(s) = \frac{s^2CL+1}{s^2CL+sCR+1} \quad (12)$$

$$H(s) = \frac{s^2+\frac{1}{LC}}{s^2+\frac{sR}{L}+\frac{1}{LC}} \quad (13)$$

This second-order transfer function contains two zeros located on the jω-axis at $\pm j\frac{1}{\sqrt{LC}}$, which create a notch response. Looking at the denominator of (13), and with the knowledge that entirely real poles create the desired response, the poles of the transfer function are found at $\frac{-1}{\sqrt{LC}}$. This corresponds to a critically damped system.

Note that this symmetric arrangement of zeros (Figure 6a) produces a symmetric response, meaning that the filter provides an identical response for both "positive" and "negative" frequencies; in other words, this exhibits non-complex filter properties.

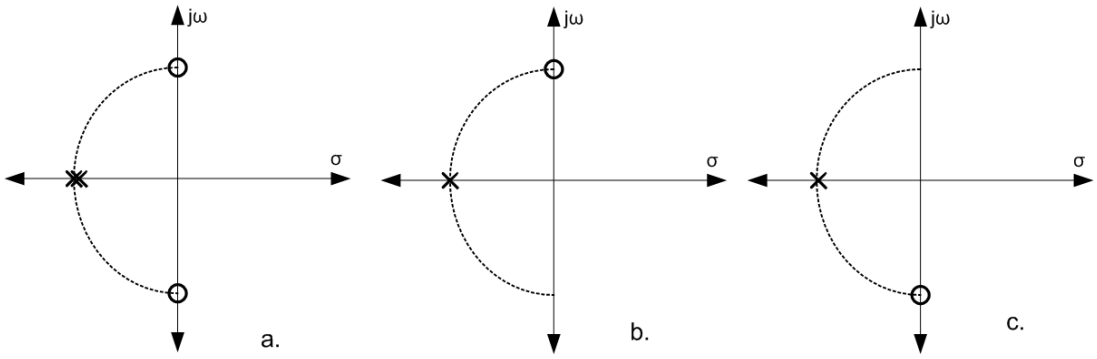

Figure 6. (a) symmetric pole-zero plot, RLC notch filter, (b) single real pole and imaginary zero, asymmetrical response, (c) single real pole and negative imaginary zero, asymmetrical response

In his 1973 Paper, "Single Sideband Modulation using Sequence Asymmetric Polyphase Networks", Gingell introduces a filter topology (Figure 7) which implements a single real pole and single negative imaginary zero (Figure 6c, Figure 6b) [4].

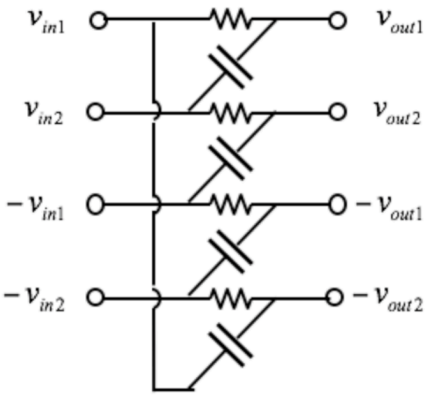

Figure 7. Gingell's RC ladder network

The equations below describe the relationships between the inputs and outputs:

$$V_{out1} = \frac{1}{sCR+1}V_{in1} + \frac{sCR}{sCR+1}V_{in2} \quad (14)$$

$$V_{out2} = -\frac{sCR}{sCR+1}V_{in1} + \frac{1}{sCR+1}V_{in2} \quad (15)$$

When combined, equations (14) and (15) produce a single transfer function in matrix form:

$$\begin{bmatrix} V_{out1} \\ V_{out2} \end{bmatrix} = \begin{bmatrix} \frac{1}{1+j\omega/\omega_o} & \frac{j\omega/\omega_o}{1+j\omega/\omega_o} \\ -\frac{j\omega/\omega_o}{1+j\omega/\omega_o} & \frac{1}{1+j\omega/\omega_o} \end{bmatrix} \times \begin{bmatrix} V_{in1} \\ V_{in2} \end{bmatrix} \quad (16)$$

This transfer function implements a single real pole and single imaginary zero when a pair of quadrature signals drive the circuit. Because of the asymmetry along the jω-axis, the filter displays an asymmetric response as well. In other words, this filter exhibits a different response based on the sign or phase difference of the input signals, i.e. a complex filter response. Gingell's RC ladder network accepts four inputs, however two of these equate to 180˚-shifted versions of the other two. In addition, V_{in2} is the same as V_{in1} shifted by 90˚; in other words, V_{in1} and V_{in2} represent a complex pair of signals. Because of these properties, this network characterizes as both differential and complex.

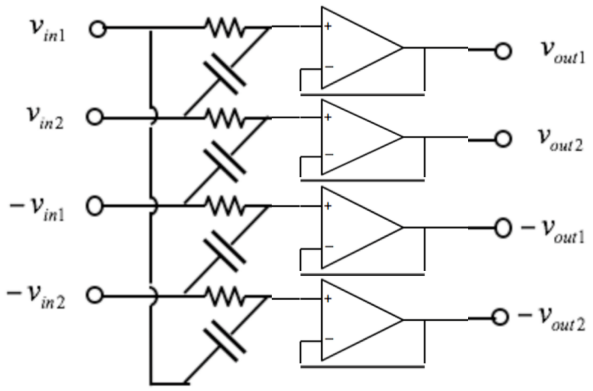

Figure 8. Directly buffered Gingell topology

As discussed in the literature review, the complex response of this filter finds uses in a variety of fields, however, in some cases, the desired frequency range of complex response proves wider than the network can provide. In this case, "cascading" provides the desired response [7]. For passive networks (Figure 7), cascading shifts

the pole location. Buffering the output resolves this issue; unfortunately buffering the circuit shown in Figure 7 requires four buffers, one for each output, for each individual network (referred to as a "stage") cascaded. With the goal of reducing the total number of active components, because two of the inputs are inverted versions of the other two, the network simplifies to only two inputs by adding an inverting stage internal to the network (Figure 9).

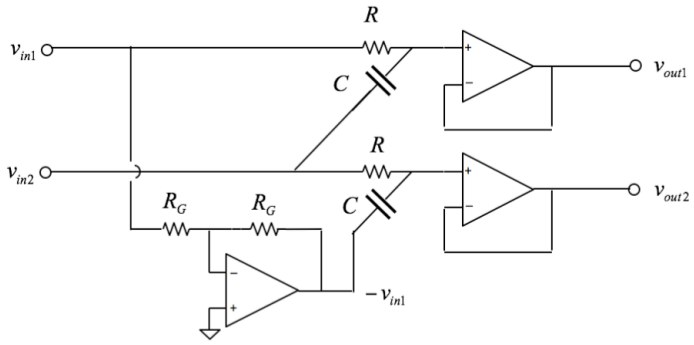

Figure 9. Simplified, Buffered, Gingell topology (2-input)

Further reduction of the number of active components follows in Section 3 "Type-II Topology".

2. LITERATURE REVIEW

2.1 Image Rejection Application

The complex filter finds use in image rejection signal processing [11]. Larrowe's paper on band-pass quadrature filters discusses the use of quadrature filters for the use of image rejection [12].

2.2 Phase-Splitting Application

The complex filter also operates as a phase-splitter or quadrature-generator. Darlington discussed this application in 1950 [13]. Saraga presents a general topology for using two phase-shift networks to create a single-sideband modulator [14]. Howard examines the subject of single-sideband methods in amateur radio applications [15]. Gingell references the popularity of complex networks for single-sideband generation and discusses the idea of the alternative of quadrature modulation [4]. Another existing topology introduces the use of a single complex lowpass filter as a substitute for the two phase-shift network mentioned previously [16].

2.3 The Hilbert Transform

The Hilbert transform is the equivalent operation of a phase-splitter. Papers by Feldman, Johansson, and Liu discuss the properties and applications of the Hilbert transform [17] [18] [19]. Hsu considers the application of the Hilbert transform for finding instantaneous frequency and introduces a new method, the "osculating circle" method [20]. The Hilbert transform also finds applications in the medical area of processing electroencephalography (ECG) readings [21].

2.4 Passive Implementations

Existing passive implementations of complex filters are some of the older incarnations of phase-splitting circuitry. In his 1955 "Realization of constant phase difference", Bell Labs' Darlington discusses a passive all-pass structure that creates a constant phase shift [13]. Saraga discusses alternatives to this all-pass structure in his "Wide-band phase splitting networks" [14]. Bedrosian builds on the LC networks presented in Darlington and Saraga's work to provide normalized design curves for the LC all-pass network [22]. Both Darlington and Saraga's topologies rely on the use of inductors; Howard presents a RC network [15]. Gingell presents a four-input, four-output passive polyphase network (the main basis for this thesis) [4].

2.5 Active Implementations

Active implementations of complex filters appear in both in older and newer applications. Larrowe presents an active implementation of a complex bandpass filter [12]. Wiebach presents design analysis of several existing active and passive implementations in addition to an investigation on the effects of component tolerances [23]. Hutchins discusses three active all-pass phase splitting networks: Lloyd's All-Pass, Budak's All-Pass, and the State Variable All-Pass [24]. Stikvoort also discusses the implementation of a polyphase filter with op-amps [25].

3. TYPE-II TOPOLOGY

3.1 Derivation

This section presents the cascadable 1st order complex filter structure, "type-II" topology. The topology consists of a pair of dual-input structures for which deriving the transfer function requires the application of superposition. Figure 10 shows a two-input topology that realizes a highpass response with respect to V_{in1} and a lowpass response with respect to V_{in2}.

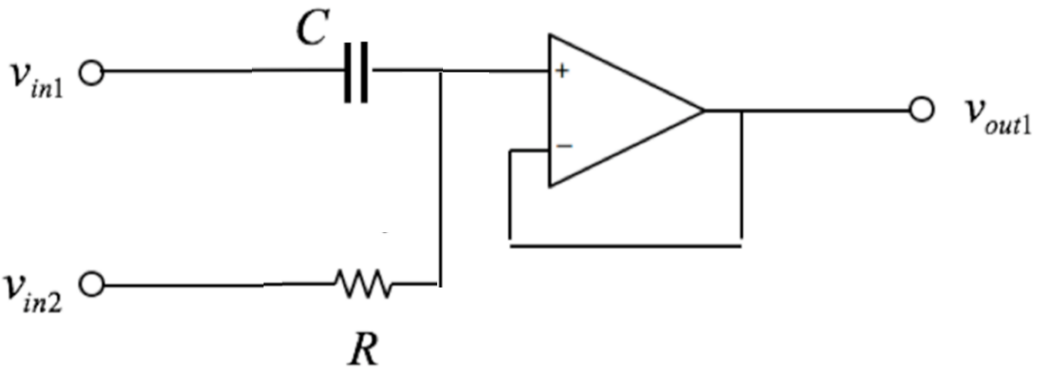

Figure 10. Active highpass/lowpass structure (non-inverting)

Superposition reveals the relationship between the inputs and outputs:

$$H_1 = \frac{V_{out1}}{V_{in1}} = \frac{sCR}{sCR+1} \quad (17)$$

$$H_2 = \frac{V_{out1}}{V_{in2}} = \frac{1}{sCR+1} \quad (18)$$

$$V_{out1} = \frac{sCR}{sCR+1}V_{in1} + \frac{1}{sCR+1}V_{in2} \quad (19)$$

Altering the above structure to utilize both of the operational amplifier's inputs (Figure 11) maintains a high pass response on the output with respect to the positive terminal (V_2) and builds an inverting low pass response with respect to the negative terminal (V_1).

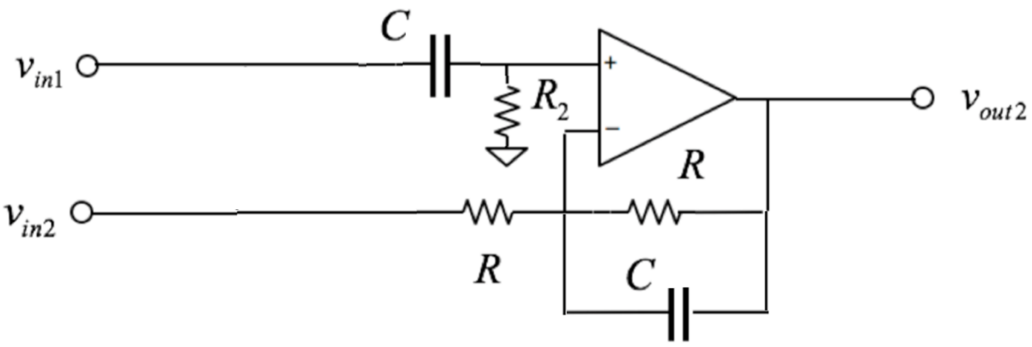

Figure 11. 2-input topology realizes inverting LP TF with respect to v1 and non-inverting HP with respect to v2

The transfer characteristics below derived again by use of superposition:

$$H_1 = \frac{V_{out2}}{V_{in1}} = \frac{sCR}{sCR+1} \quad (20)$$

$$H_2 = \frac{V_{out2}}{V_{in2}} = \frac{-1}{1+sCR} \quad (21)$$

$$V_{out2} = \frac{sCR}{1+sCR} V_{in1}(s) + \frac{-1}{1+sCR} V_{in2}(s) \quad (22)$$

The circuit shown in Figure 11 is not complex on its own, but it can replace the inverter and buffer (and adjacent circuitry) preceding V_{out2} in Figure 9; this results in the topology in Figure 12.

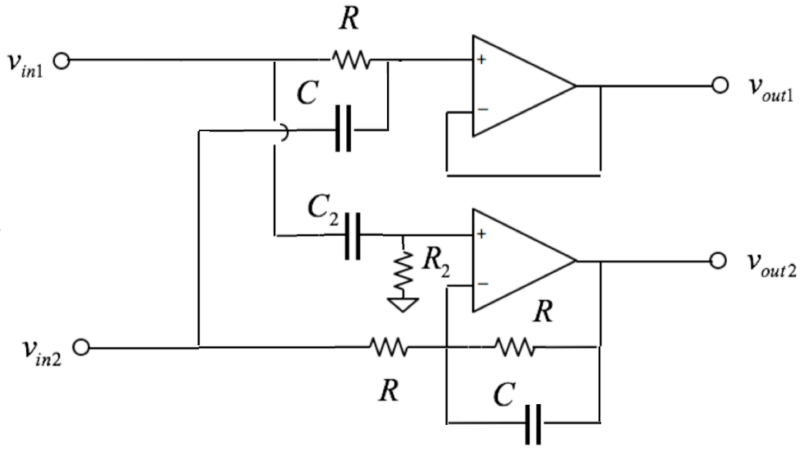

Figure 12. "Inverting" topology

This complex filter has the same transfer function magnitude as Gingell's RC network (Figure 7, equations (14) and (15)) if $C_2 = C$ and $R_2 = R/2$. LTspice testing confirmed the filter's performance (Figure 13). The filter components set a center frequency of 3.162kHz.

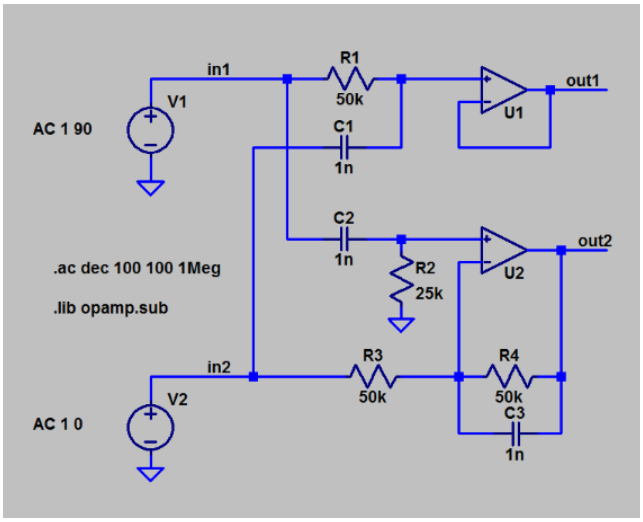

Figure 13. Single-stage complex filter

Setting V_1 *to* a cosine function and V_2 to a negative sine function produces a notch response on both outputs (Figure 14). Note that the V_{out1} responses (in red) lies exactly underneath the V_{out2} responses (in blue) in both Figure 14 and Figure 15.

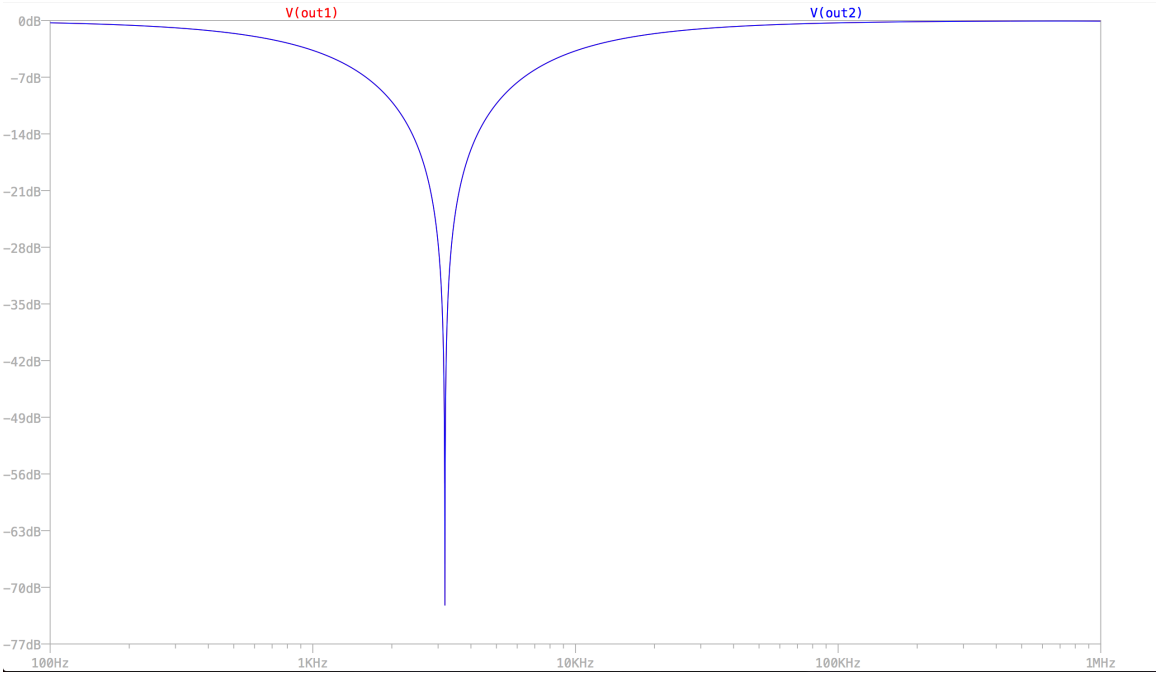

Figure 14. Inputs: COS, -SIN produces a notch at f_C= 3.162kHz

Setting V_1 *to* a cosine function and V_2 to a sine function produces a bandpass response on both outputs (Figure 15); note that once again, the two responses lie on top of each other.

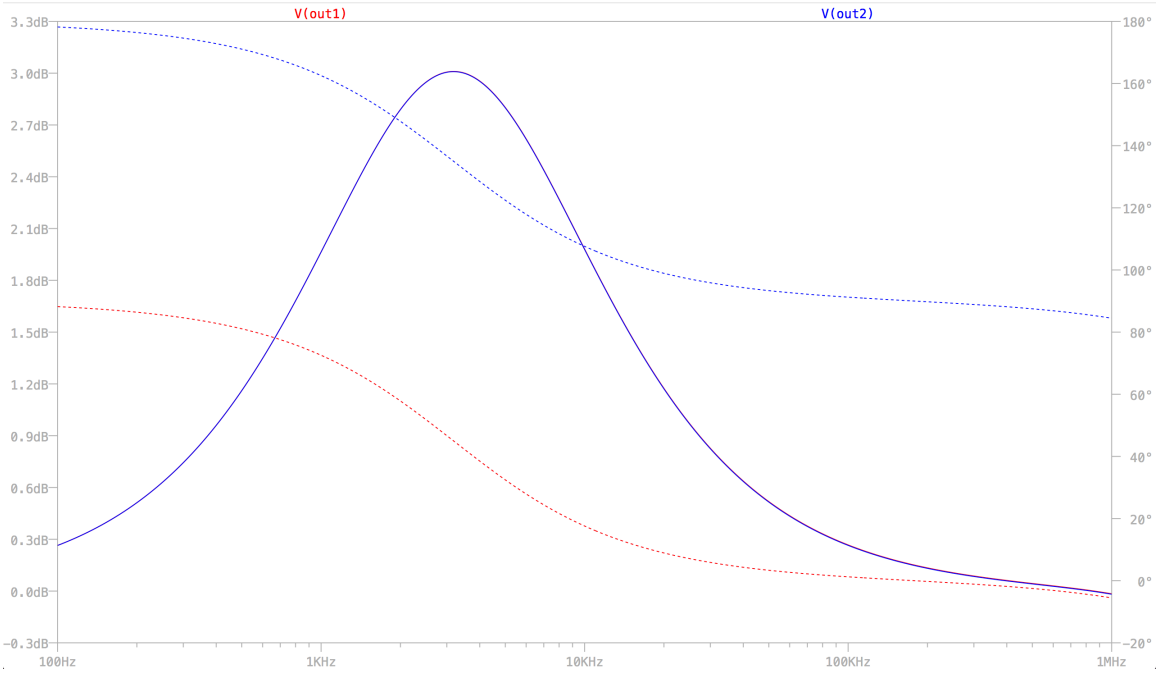

Figure 15. Inputs: COS, SIN, produces a bandpass at f_C= 3.162kHz

Setting V_1 and V_2 to the same cosine function produces neither the notch response nor the bandpass response; this produces an all-pass response (Figure 16). Observe that the nearly constant magnitude response, however, the phase response of the second output varies.

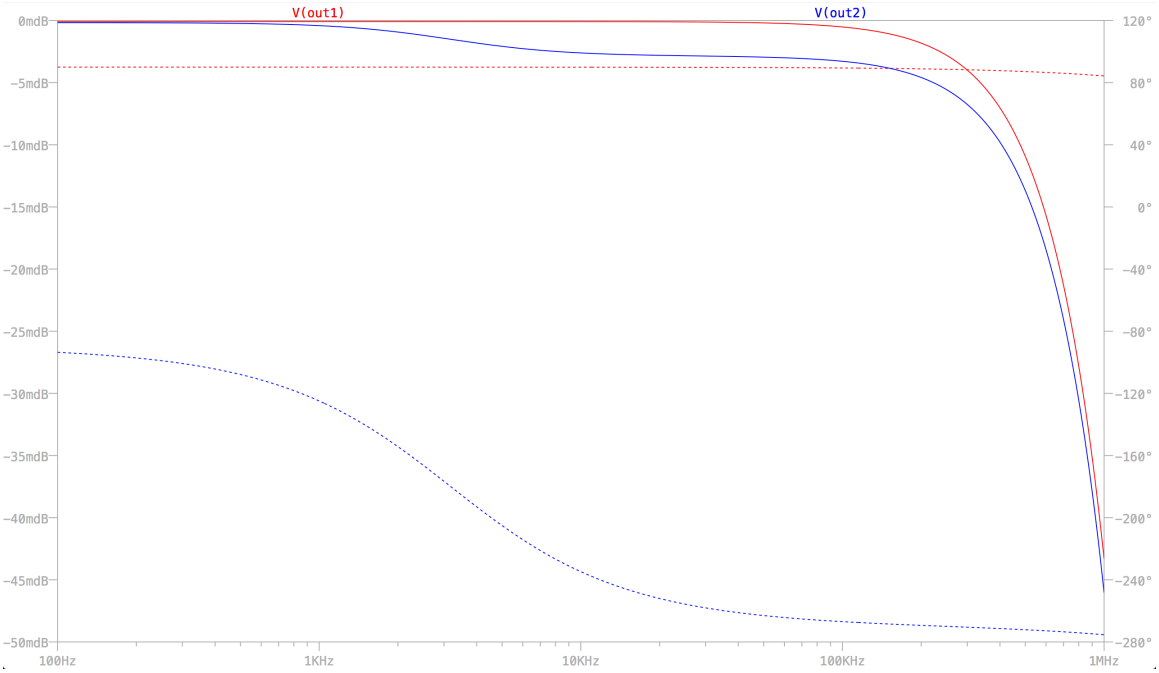

Figure 16. Inputs: COS, COS produces an all-pass circuit

Setting V_2 *to* ground and V_1 to a 3.162kHz sine function produces a sinusoid response on both outputs (Figure 17). Note that the outputs shift approximately 90˚ out of phase with each other and V_{out1} magnitude equals V_{in1} magnitude.

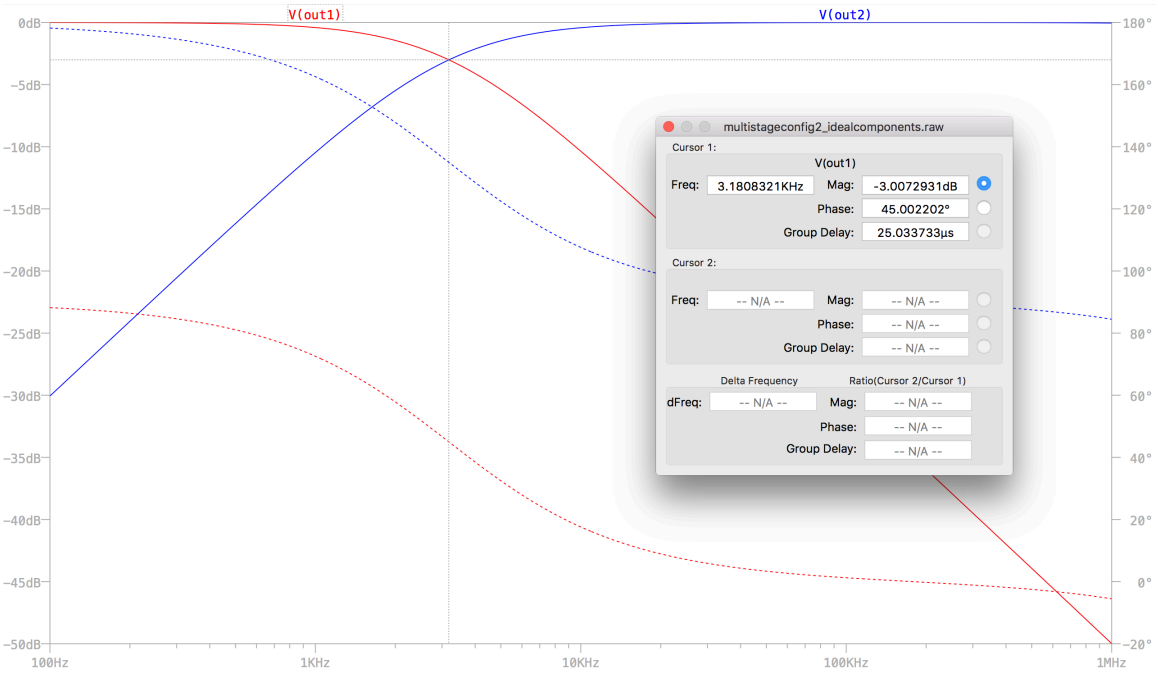

Figure 17. Frequency domain analysis of circuit in Figure 4: produces a 90° phase difference, V_{in1} a 3.162kHz signal, V_{in2} grounded

The above confirms the topology's functionality as both a positive and negative frequency discriminator and as a quadrature signal generator. Note that as a phase splitter, the magnitude of the quadrature outputs is only the same at the designed center frequency. Generating quadrature over a wider range requires higher-order networks.

3.2 Cross-coupling

This section returns to the original intent of designing a cascadable topology for the purpose of creating broadband frequency responses. To cascade multiple stages, first notice the sign change in V_{out2} with respect to V_{in1} and V_{in2} (Table 1).

Table 3. Comparison of Gingell's and Type II transfer functions

Original Gingell	**Type II Inverting**
$\mathrm{V_{out1}} = \frac{1}{\mathrm{sCR}+1}\mathrm{V_{in1}} + \frac{\mathrm{sCR}}{\mathrm{sCR}+1}\mathrm{V_{in2}}$	$V_{out1} = \frac{1}{sCR+1}V_{in1} + \frac{sCR}{sCR+1}V_{in2}$
$\mathrm{V_{out2}} = -\frac{\mathrm{sCR}}{\mathrm{sCR}+1}\mathrm{V_{in1}} + \frac{1}{\mathrm{sCR}+1}\mathrm{V_{in2}}$	$V_{out2} = \frac{sCR}{sCR+1}V_{in1} - \frac{1}{1+sCR}V_{in2}$

Because of this sign change, it is necessary to "cross couple" by connecting V_{out1} of the stage to V_{in2} of the next stage and V_{out2} *of* the stage to V_{in1} of the next stage. This introduces an additional 180˚ phase shift, which equates to a negative sign; this corrects the sign change in overall transfer function of the cascaded filter. See the appendix for a full explanation on Gingell response to positive and negative sequences.

The figures below show the results of cross-coupling and not cross-coupling in different forms, proving the necessity of cross-coupling to maintain the desired system response. Figure 19 and Figure 20 demonstrate the results of cross-coupling, while Figure 23, Figure 26, and Figure 27 show the undesired response that occurs without cross-coupling.

Figure 19 shows the result of cross-coupling the stages to each other. The response after each stage shows the results of the cascaded preceding stages building upon each other. From Figure 20, note that cross-coupling keeps the zeros (corresponding to the notches in the frequency response) on the negative portion of the frequency axis.

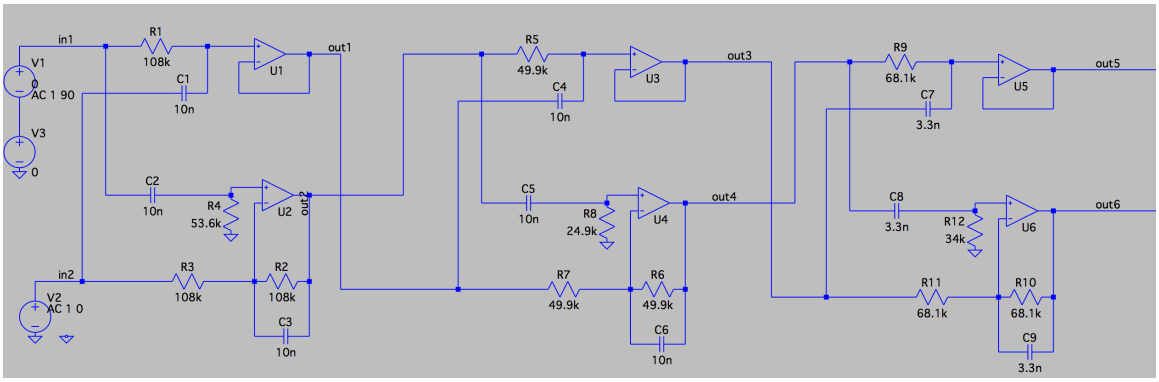

Figure 18. Cross-coupling all stages, schematic

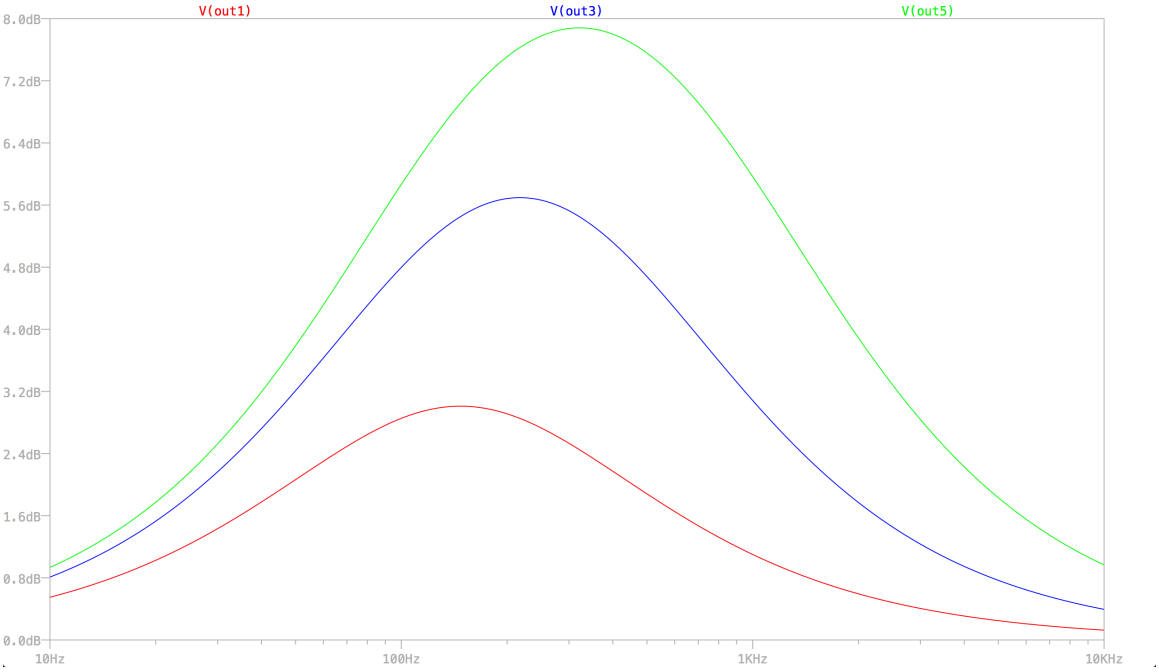

Figure 19. Cross-coupling all stages, simulation response

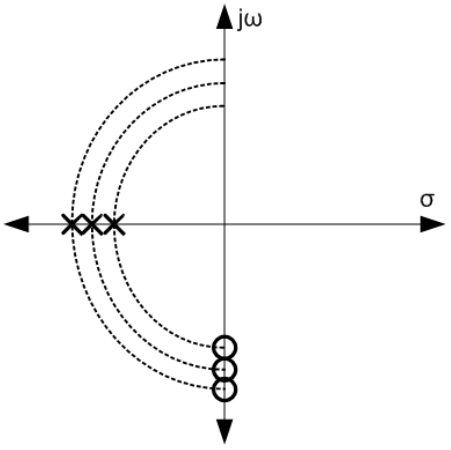

Figure 20. S-plane plot of three-stage filter, cross-coupled

Not cross-coupling a stage (in this case, just the connection between the first and second stages) results in a sign change of the location of the zeros. Figure 21 shows the s-plane plot, demonstrating how the zeros of the stages after the non-cross coupled stage change sign. Figure 23 shows the simulated response.

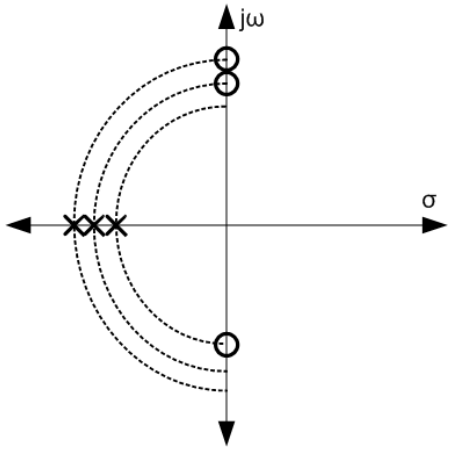

Figure 21. S-plane plot of three-stage filter, second stage not-cross coupled

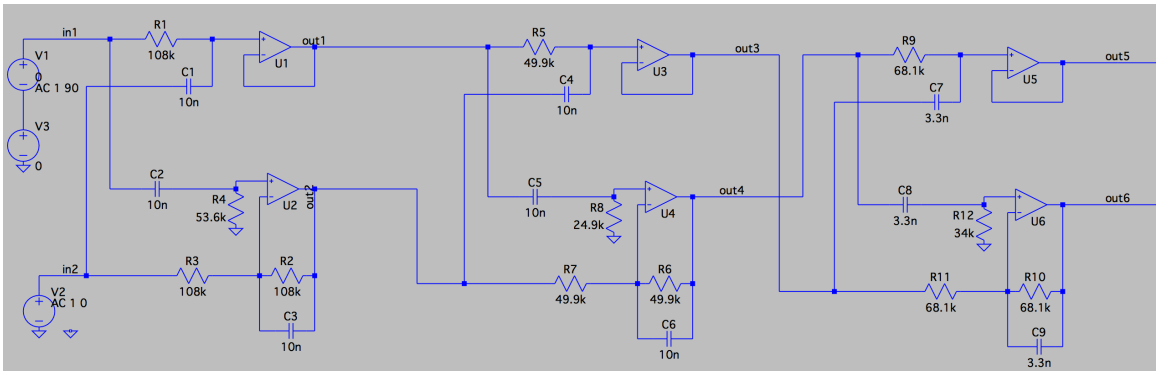

Figure 22. No cross-coupling between first and second stage, schematic

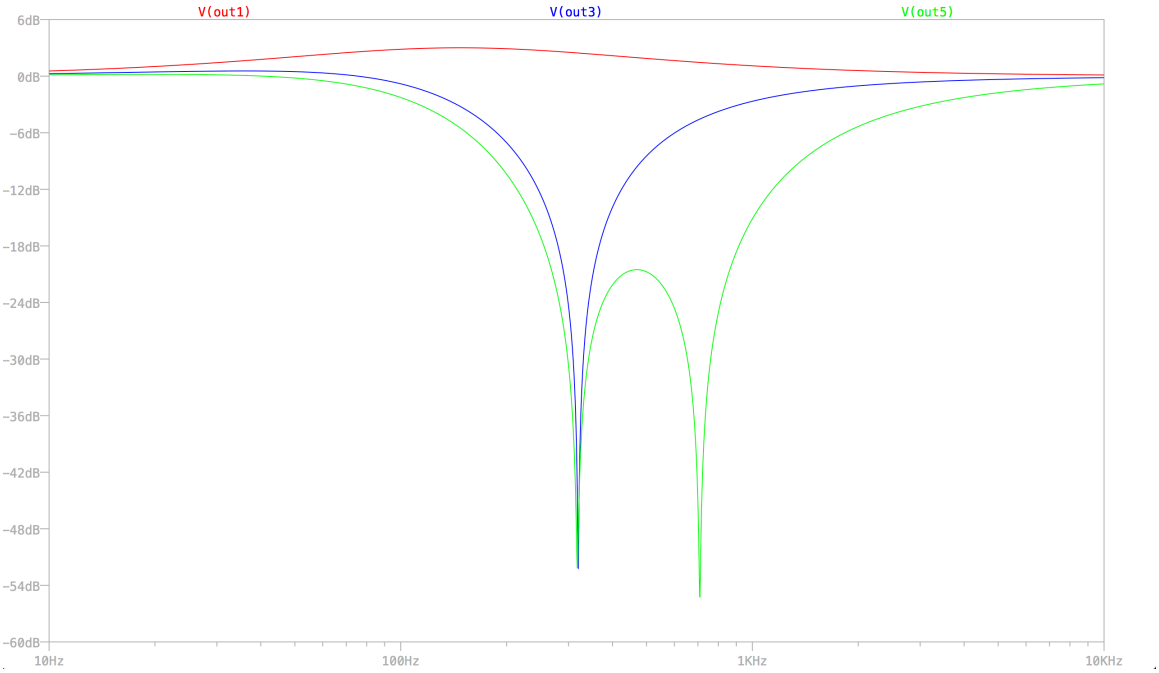

Figure 23. No cross-coupling between first and second stage, simulation response

Not cross-coupling all the stages cause the sign of the zeros to alternate with respect to adjacent frequencies (Figure 24).

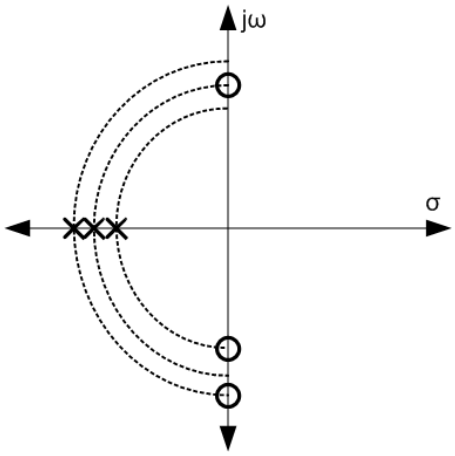

Figure 24. S-plane plot of three-stage filter, all stages not-cross coupled

The figures below show the simulation results of not cross-coupling any stages. Figure 26 shows the response of a three-stage filter, and Figure 27 shows the response of a five-stage filter.

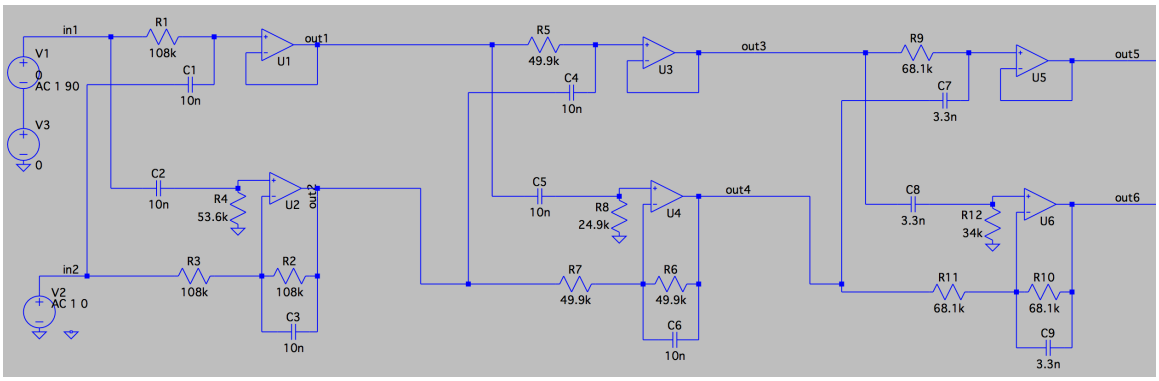

Figure 25. Three-stage filter, all stages not cross-coupled, schematic

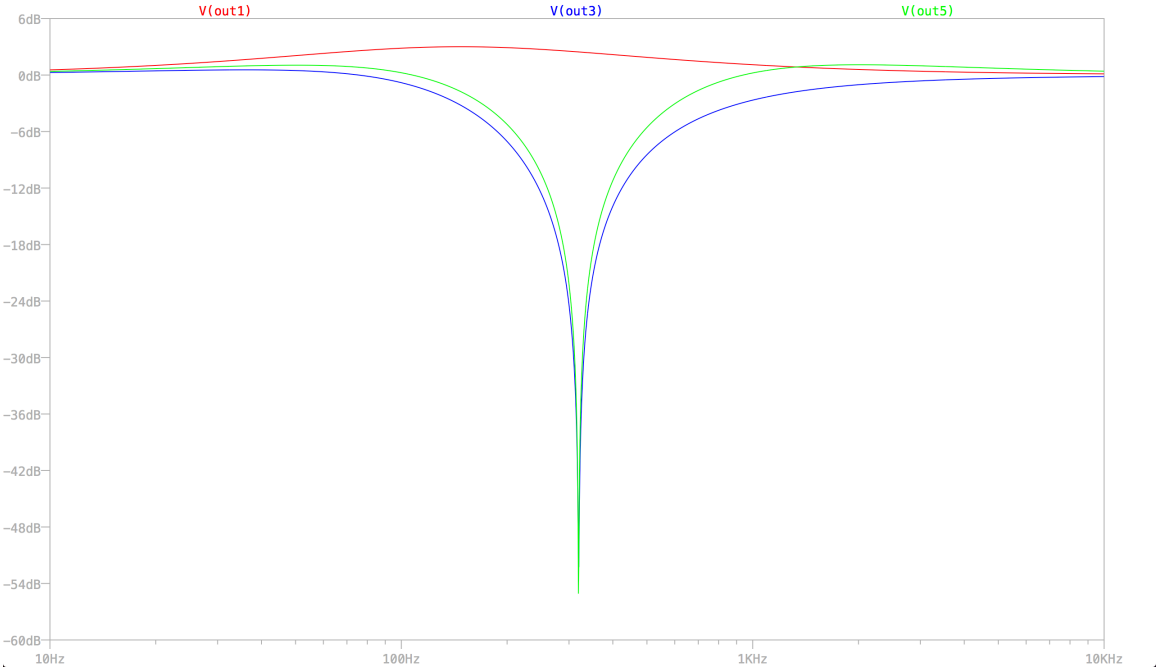

Figure 26. Three-stage filter, all stages not cross-coupled, simulation response

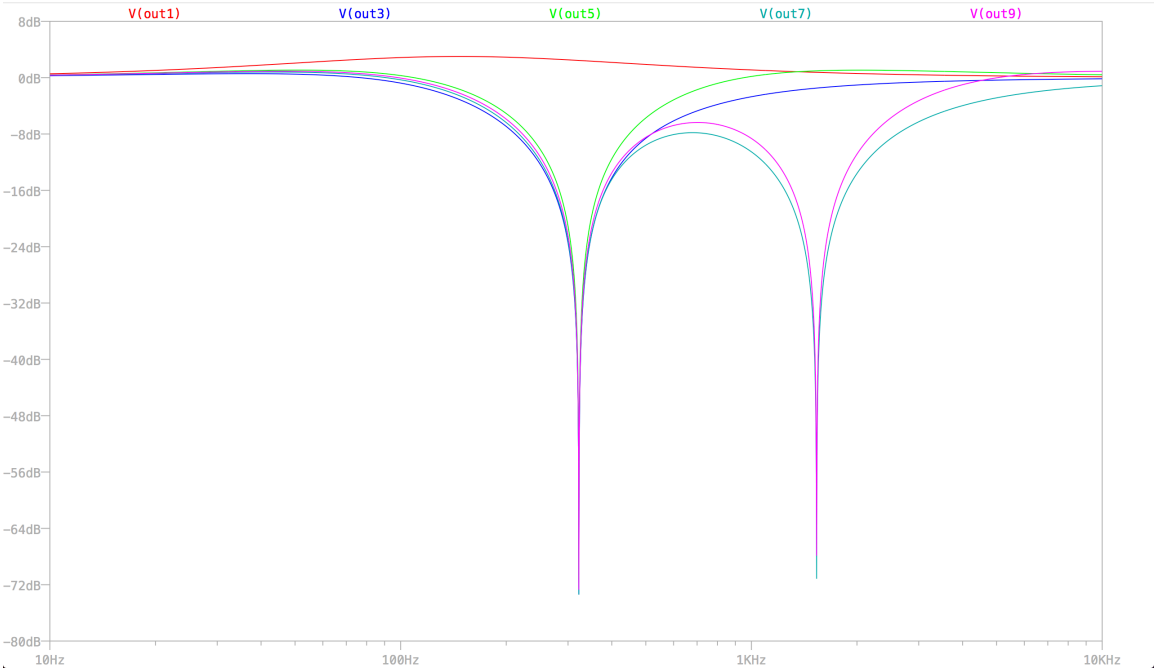

Figure 27. Five-stage filter all stages not cross-coupled, simulation response

3.3 Design Example

The following design example demonstrates the performance of a 5-stage filter and the effects of component matching and tolerances in addition to the construction of a prototype filter. The method used for determining the notch frequency for each stage involves placing each notch equidistantly in a log scale along the frequency range of interest. Such placement results in near equi-ripple stopband characteristics. This example uses a notch spacing ratio of $k = 2.18$.

Table 4. Notch frequency values

	Frequency (Hz)
$\mathbf{f_1}$	147
$\mathbf{f_2}$	322
$\mathbf{f_3}$	703
$\mathbf{f_4}$	1534
$\mathbf{f_5}$	3344

Figure 28 is a schematic of the five filter stages.

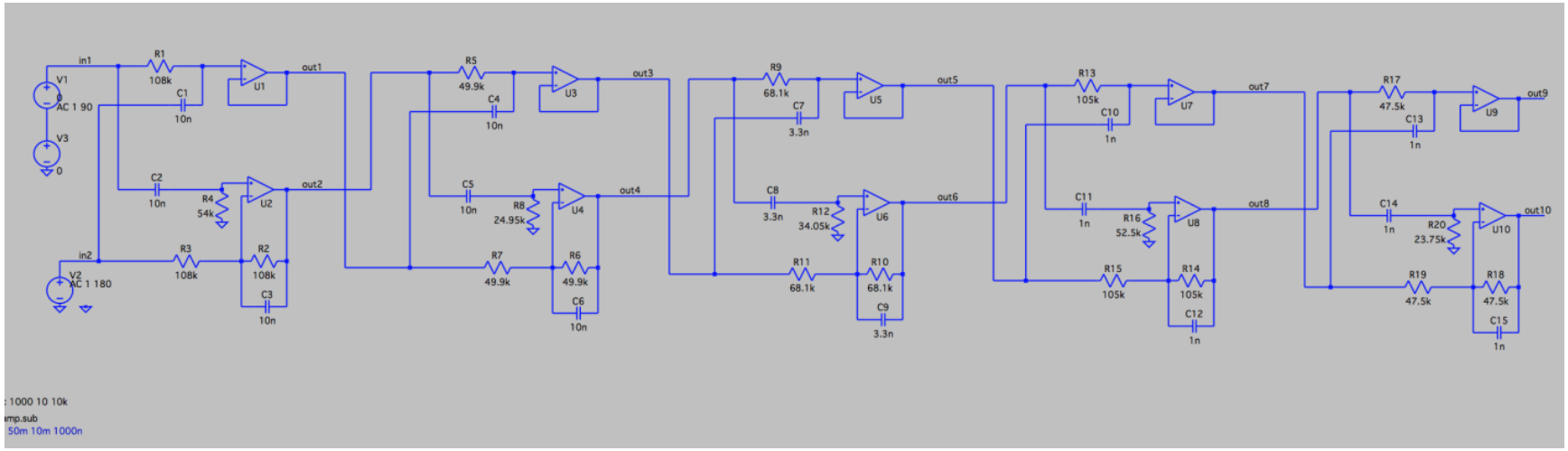

Figure 28. Inverting topology, 5 stages cascaded, ideal component values

Using the equation for the RC time constant and choosing reasonable values for the capacitor ($C_{stage1} = C_{stage2} = 10nF$, $C_{stage3} = 3.3nF$, $C_{stage4} = C_{stage5} = 1nF$), Table 5 shows the calculated resistor values for each stage (corresponding to each stage frequency). Figure 29 shows the results of the simulation with ideal component values.

Table 5. Ideal values for each stage of inverting topology

Resistor	**Stage 1**	**Stage 2**	**Stage 3**	**Stage 4**	**Stage 5**
R1	108.269k	49.9k	68.604k	103.752k	47.5231k
$R2 = \frac{1}{2}R1$	54.1345k	24.7k	34.302k	51.876k	23.7616k

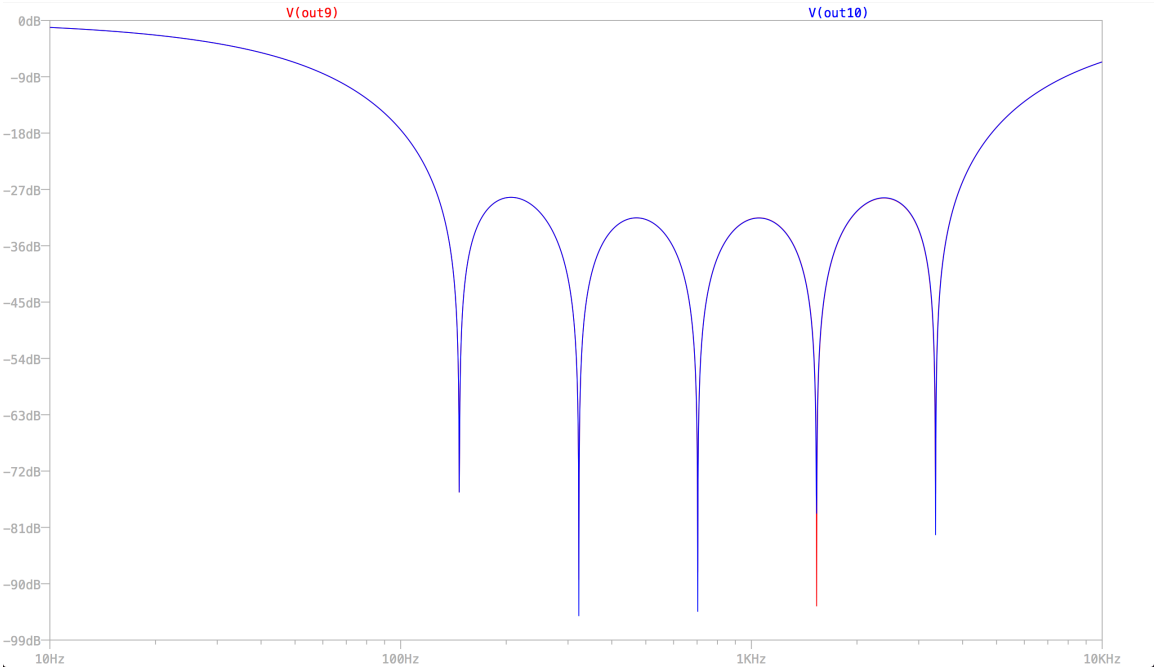

Figure 29. Stop-band performance of 5th order cascade, ideal component values

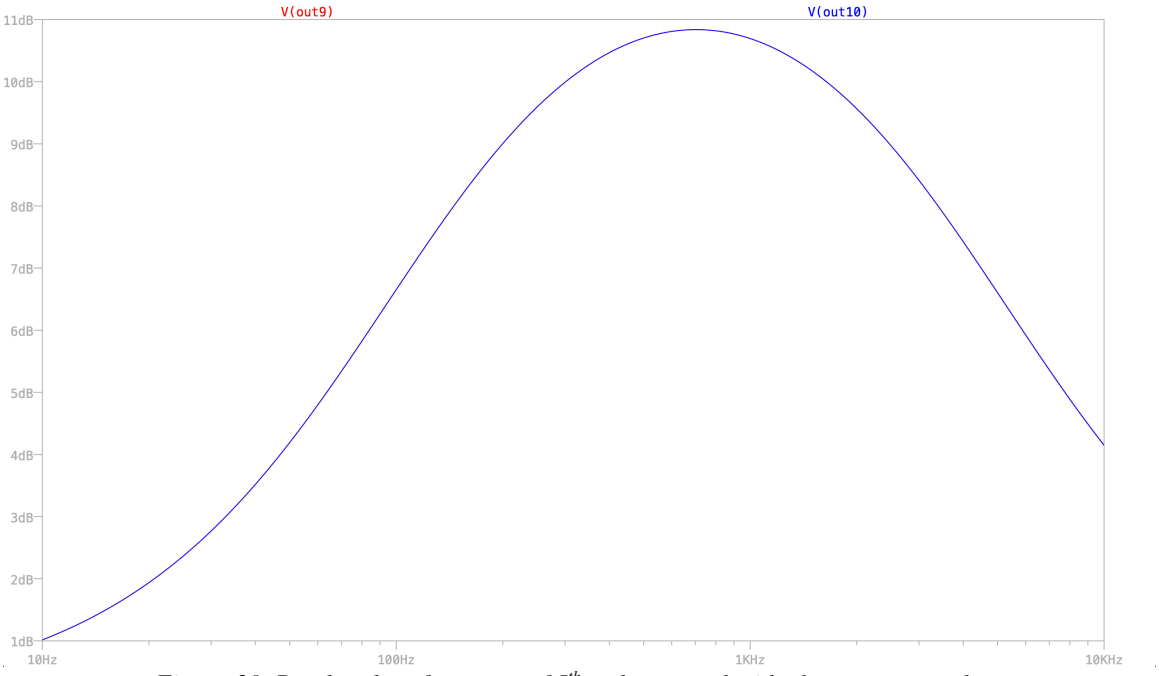

Figure 30. Passband performance of 5th order cascade, ideal component values

Rounding to standard 1% resistor values, also known as EIA E96 values, results in Table 6 [26]. Figure 31 shows the results of simulating with standard 1% values.

Table 6. E96 values for inverting topology

Resistor	**Stage 1**	**Stage 2**	**Stage 3**	**Stage 4**	**Stage 5**
R1	108k	49.9k	68.1k	105k	47.5k
R2	53.6k	24.9k	34k	52.3k	23.7k

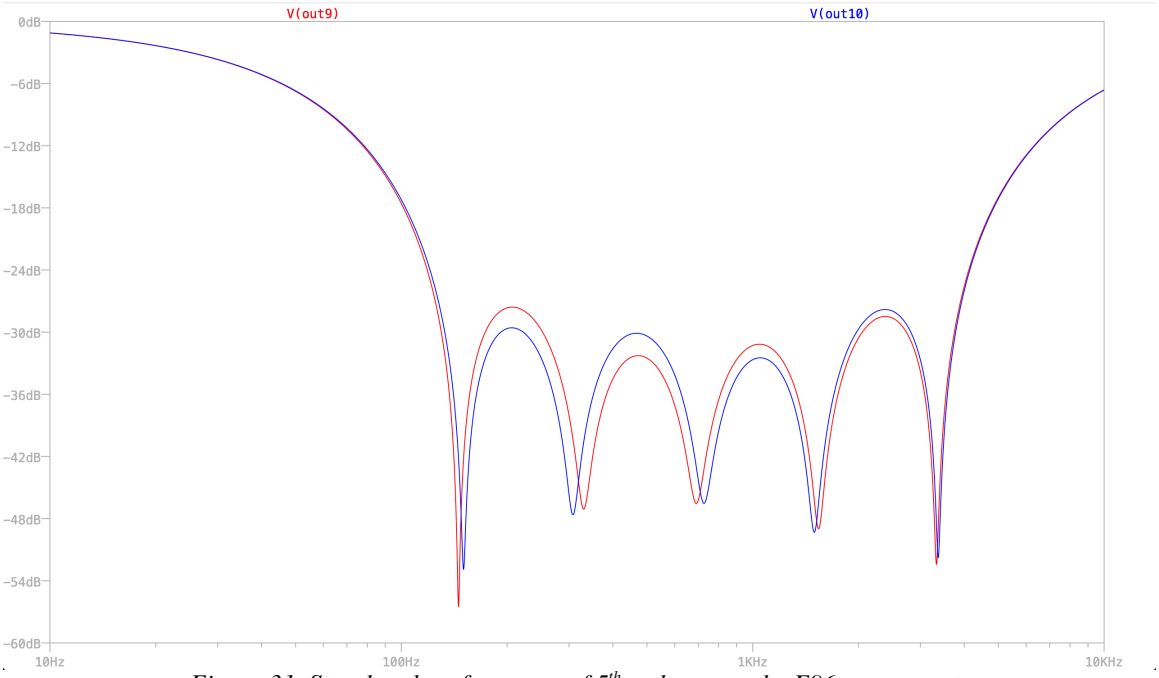

Figure 31. Stop-band performance of 5th order cascade, E96 components

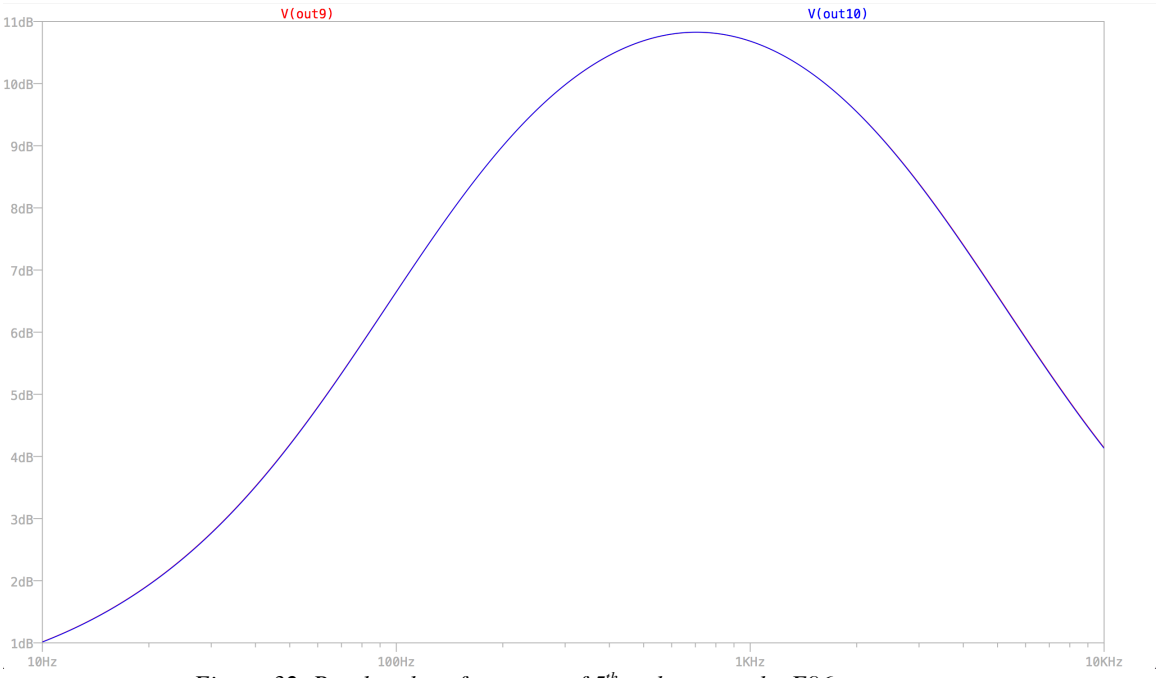

Figure 32. Passband performance of 5th order cascade, E96 components

To investigate the effects of component variation, Table 7 shows the values of R2 when calculated as a parallel combination as R1. Figure 33 shows the results of simulating with the values shown in Table 7.

Table 7. E96 values for inverting topology, R2 as a parallel combination of two R1

Resistor	**Stage 1**	**Stage 2**	**Stage 3**	**Stage 4**	**Stage 5**
R1	108k	49.9k	68.1k	105k	47.5k
R2	54k	24.95k	34.05	52.5	23.75

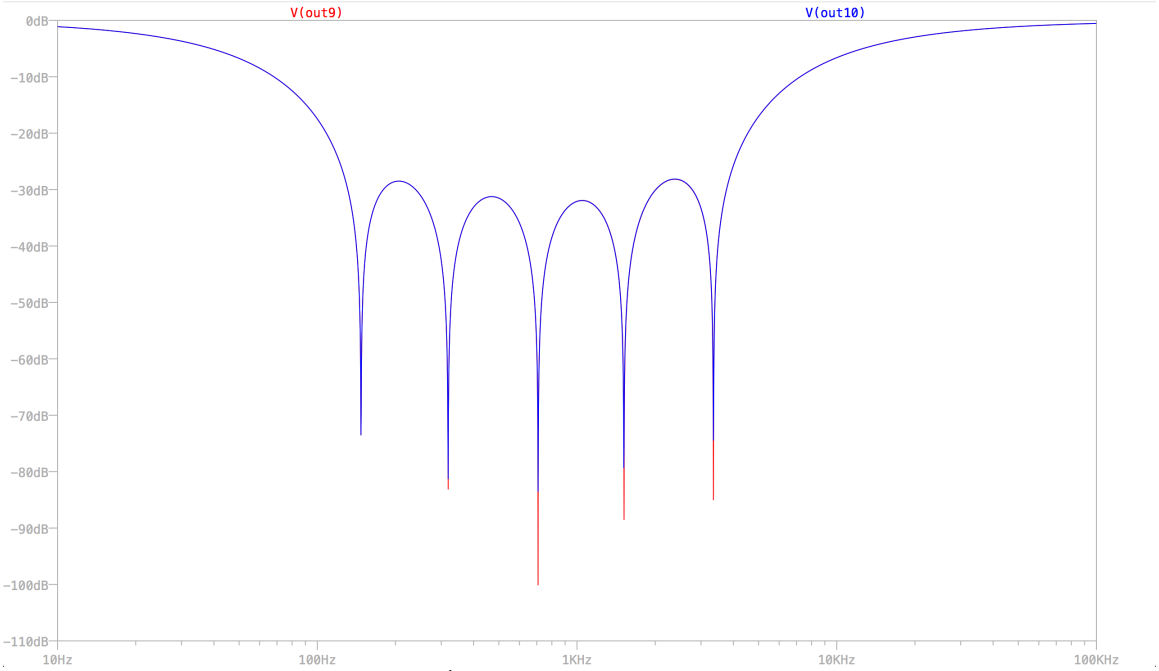

Figure 33. Stop-band performance of 5th order cascade, E96 components, R2 as parallel combination of two R1

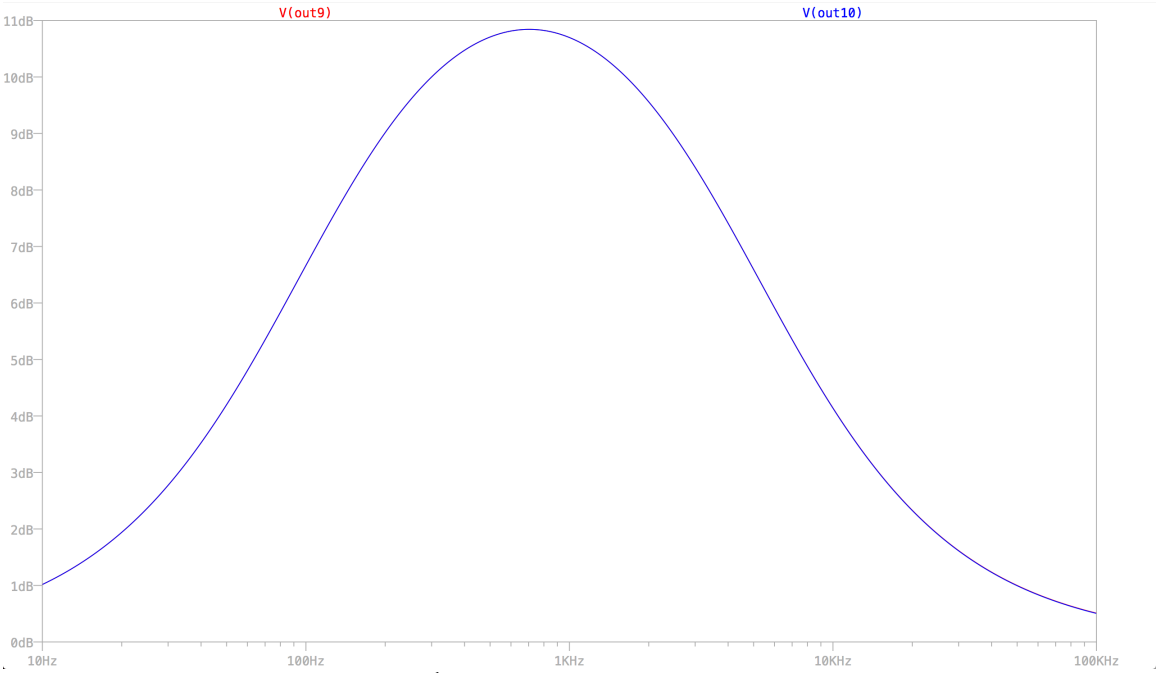

Figure 34. Passband performance of 5th order cascade, E96 components, R2 as a parallel combination of two R1

While the filter composed of standard 1% resistors for R1 and a parallel combination of R1 for R2 performed better in simulation, using the values in Table 6 perform more practically for prototyping.

Table *8* lists the prototype component values. The prototype utilizes the MCP6282 450µ*A*, 5MHz Rail-to-Rail Op Amp with a 5V supply. Figure 35 shows the prototype after building.

Table 8. Component values for design example

Stage	Notch Frequency (Hz)	Component Values	
		E96 Capacitor (nF)	*E96 Resistor (kΩ)*
1	151	10	108
2	326	10	49.9
3	700	3.3	68.1
4	1505	1.0	105
5	3236	1.0	47.5

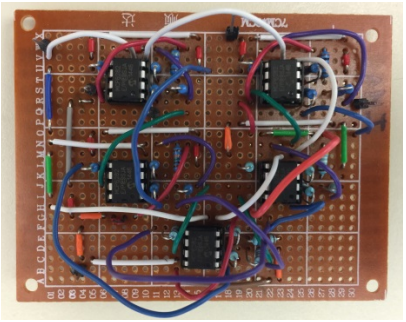

Figure 35. Fine-stage active complex filter prototype implemented using five dual MCP6282 op-amp chips on perfboard

Because of the sensitivity to component tolerances demonstrated in simulation, the prototype is constructed on perfboard to avoid the stray capacitance common with solderless breadboards. Perfboard (DOT PCB) consists of copper pads in the same standard spacing as a breadboard on a hard printed circuit board-type material.

To verify the prototype's performance as a broad-band phase-splitter, drive the filter with one input grounded and the other receiving a sinusoid signal. Measure the two filter outputs with the input signal set to the individual stage center frequencies (Figure 36). The phase difference between the two signals in each capture is approximately 90˚. The magnitudes of the two signals remain nearly the same over the large span of test frequencies.

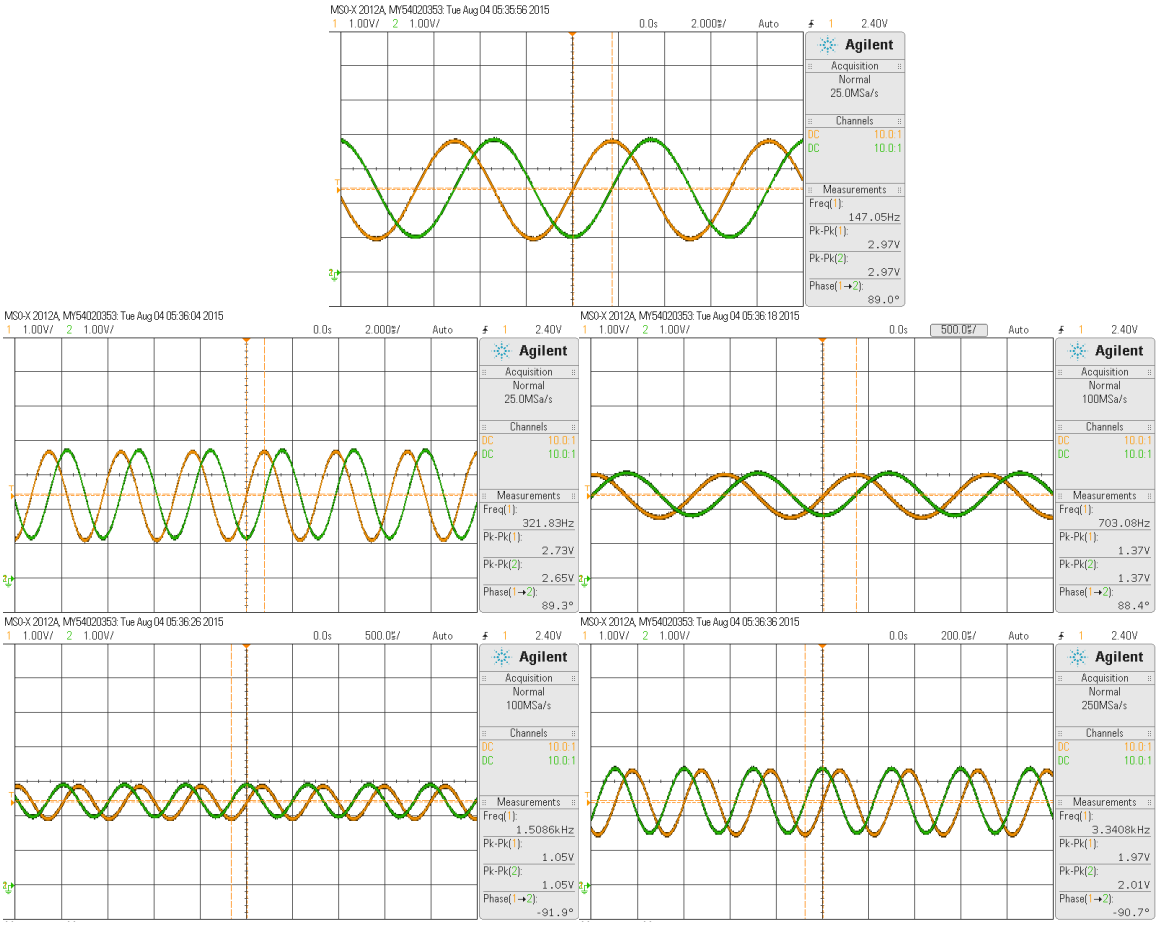

Figure 36. 5-stage design performs 90° phase-splitting for five different frequencies, (top to bottom, left to right – 147Hz, 321Hz, 703Hz, 1.508kHz, and 3.34kHz)

Using a pair of quadrature signals on the input stimulates the circuit's asymmetric frequency response (Figure 37 and Figure 38).

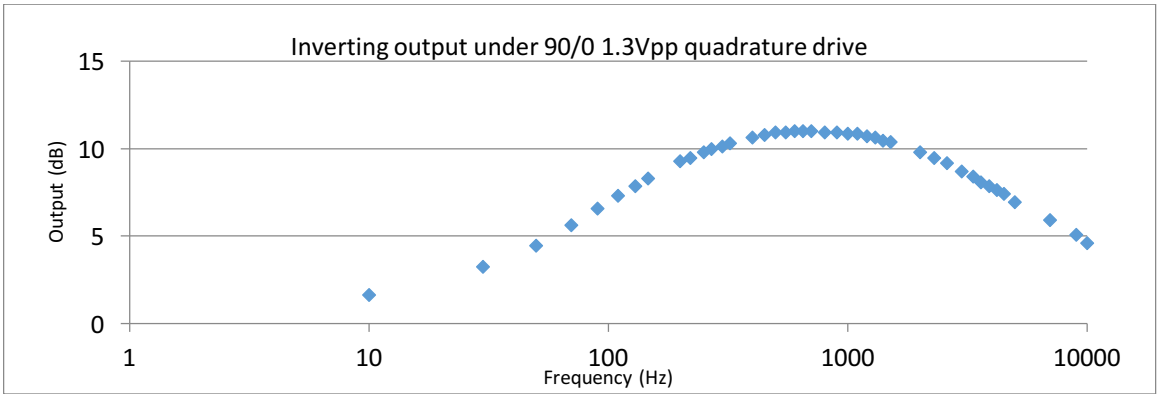

Figure 37. Filter magnitude for image-reject operation, passband

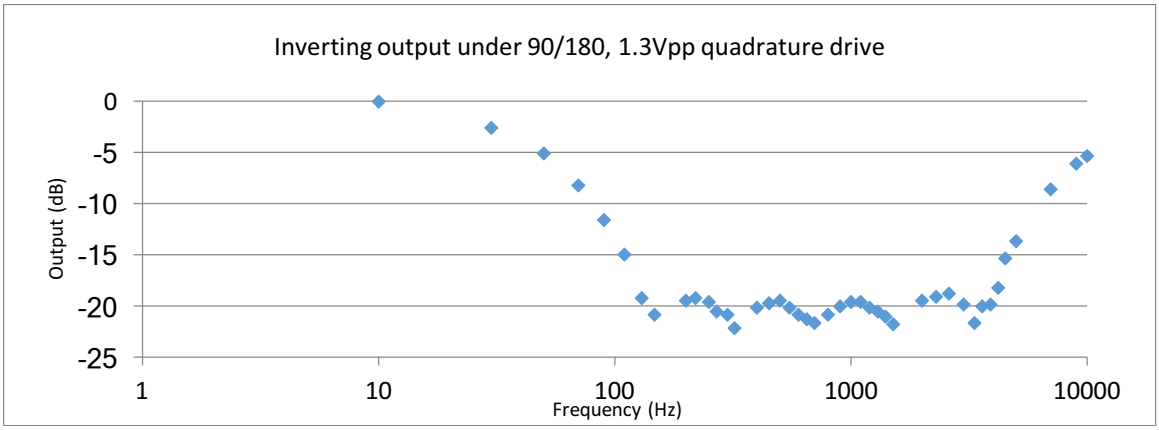

Figure 38. Filter magnitude for image-reject operation, stopband

Finally, in order to judge the performance of the prototype, key characteristics are measured and compared to simulation results and mathematical modeling (Table 9, Figure 39).

Table 9. Comparison of calculation, simulation, and measured values

	Simulation	**Measurement**
Stopband Attenuation	29.9dB	19.5dB
Peak Gain	10.8dB	11.0dB
3dB Cutoff Passband Frequencies	138Hz, 3.54kHz	130Hz, 3.70kHz
Stopband End Notch Frequencies	145Hz, 3.33kHz	147Hz, 3.42kHz

Below find figure and definitions of parameters in Table 9.

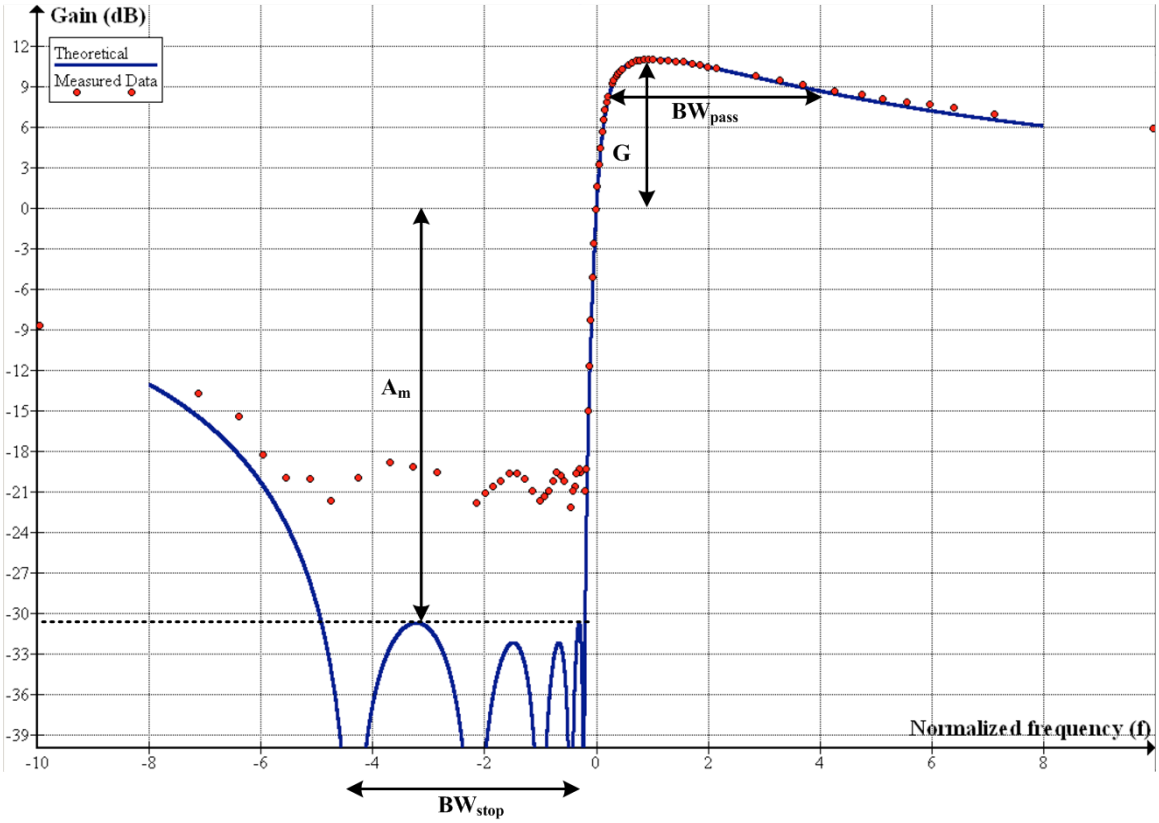

Figure 39. Plot of theoretical transfer function and measured data for 5-stage circuit

Equation 26 mathematically represents the system transfer function; Figure 39 shows the transfer function graphed along with the data points shown in Figure 37 and Figure 38 for comparison. For further explanation of the origin of this function, see chapter 4.

$$H(x) = 20\,log_{10}\left[\frac{\left|1+\frac{x}{2\times k}\right|}{\sqrt{1+\left(\frac{x}{(2\times k)}\right)^2}}\times\frac{\left|1+\frac{x}{k}\right|}{\sqrt{1+\left(\frac{x}{(k)}\right)^2}}\times\frac{|1+x|}{\sqrt{1+(x)^2}}\times\frac{|1+kx|}{\sqrt{1+(kx)^2}}\times\frac{|1+2\times kx|}{\sqrt{1+(2\times kx)^2}}\right] \quad (23)$$

To quantify the performance of a filter, first define the measurement parameters and definitions. Four main quantities describe the filter: stopband bandwidth, stopband attenuation, passband gain, and passband bandwidth. Stopband bandwidth, BW_{stop}, defines the range of frequencies in-between the filter's lowest and highest frequency notch; note that this is not a -3dB bandwidth, find the reasoning in [7].

Stopband attenuation, A_m, defines the distance from unity gain (0dB) to the highest peak within the stopband region. Passband gain, G, constitutes the maximum amount of gain in the passband response. Passband bandwidth, BW_{pass}, is a -3dB bandwidth; it defines the range of frequencies for which the magnitude response measures less than 3dB away from the passband gain, G.

Figure 39 shows roughly 12dB less attenuation in the stopband, A_m, than expected according to the mathematical model, similarly, Table 9 shows approximately 10dB less attenuation when compared to simulation results. One source of this difference comes from component tolerances. However, because the lobes in the measured response seem to follow the lobes of the expected response, imperfect quadrature drive used to test the filter could also contribute to this difference. Figure 40 below shows the effects of driving the input with signals with a 89˚ phase difference (in red) or a 88˚ phase difference (in green) instead of 90˚ (in blue). In addition, Figure 41 shows a comparison of having less than 90˚ phase difference (89˚ in red) and having more than 90˚ phase difference (91˚ in green).

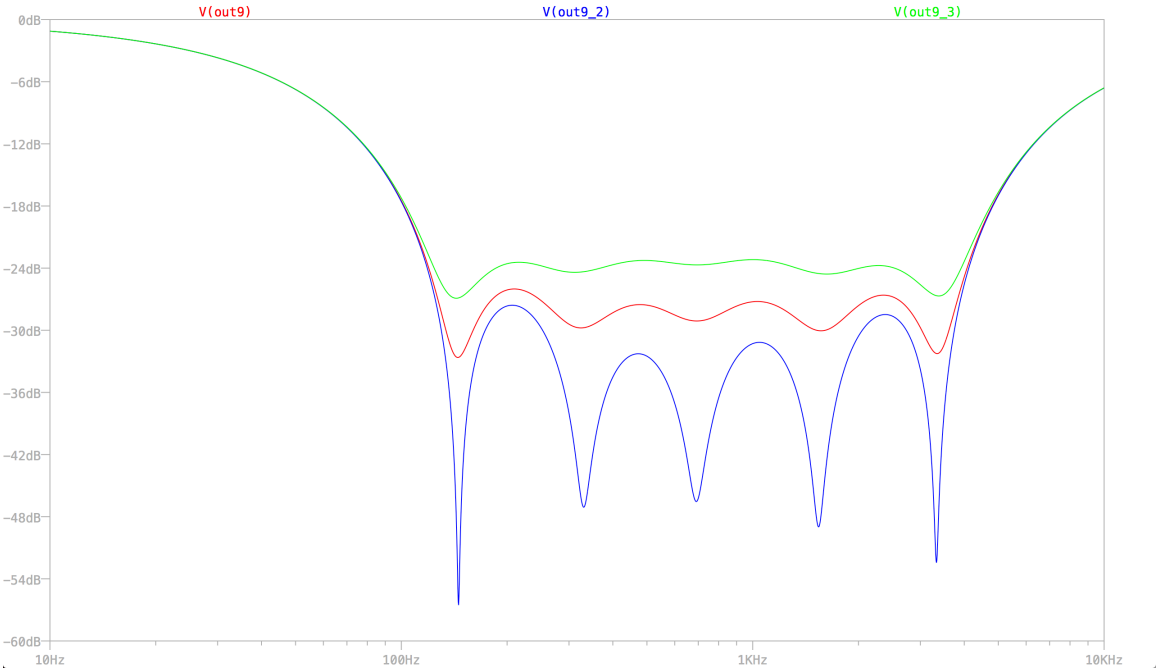

Figure 40. Simulation: driving with imperfect quadrature, 90˚(blue), 89˚(red), 88˚(green)

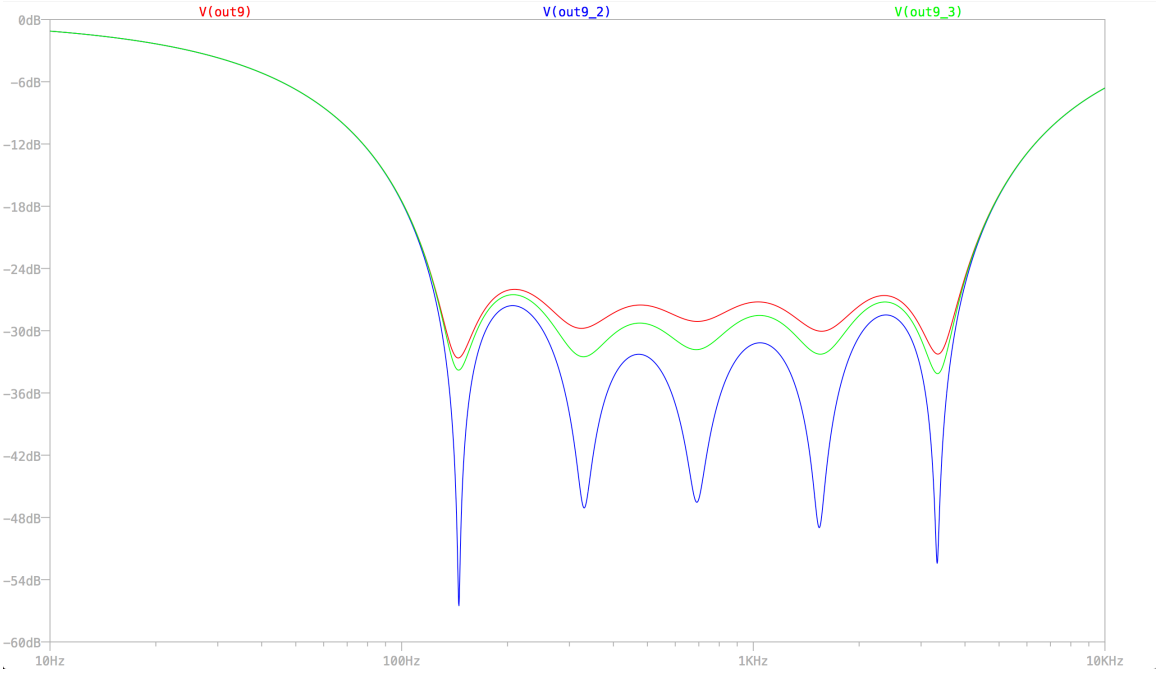

Figure 41. Simulation: driving with imperfect quadrature, 90˚(blue), 89˚(red), 91˚(green)

The above figures demonstrate the effects of driving with imperfect phase on the quadrature inputs. The source could also have variations on the voltage. The same

circuit is simulated with input sources varying 2% in magnitude (Figure 42). This shows the significant effect that driving source accuracy has on the circuit response.

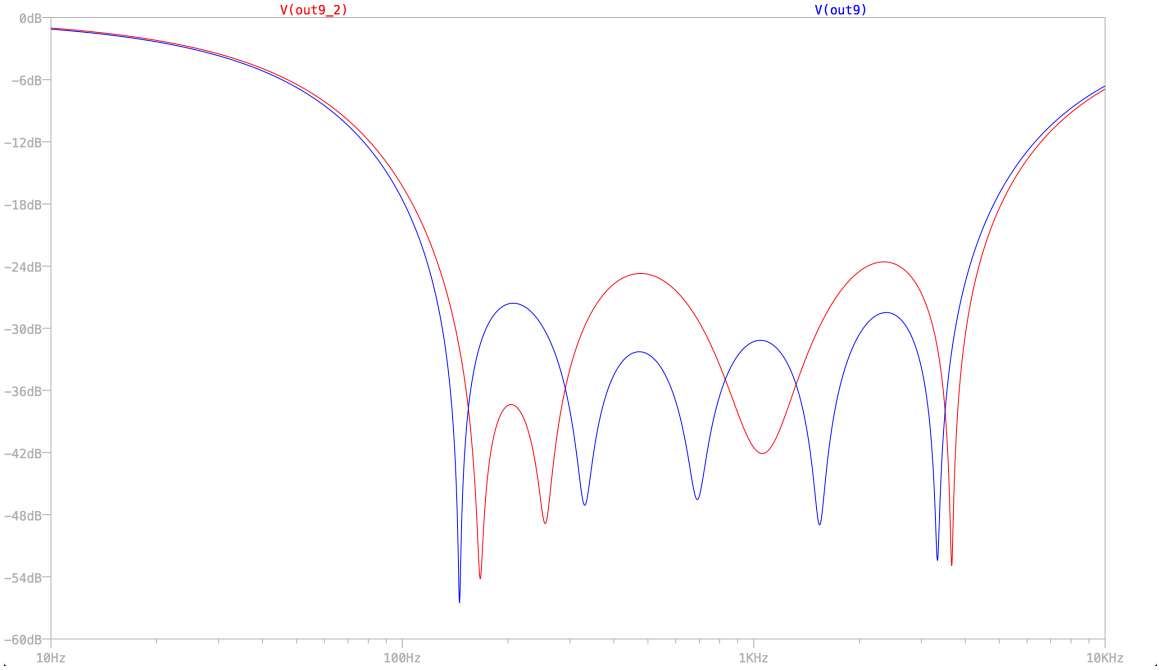

Figure 42. Simulation: driving with imperfect quadrature, 2% voltage variation (red), ideal (blue)

4. MODELING OF BAND-PASS REGION

As described in the previous section, four design constraints exist: passband bandwidth, passband gain, stopband bandwidth, and stopband gain. Only two parameters adjust directly in design: number of stages, N, and frequency spacing, k. Because of this mismatch, the design is inherently over constrained. This section explores the two passband characteristics as a function of N and k *in* an effort to provide general closed-form equations for the purpose of filter design (see Chapter 5 design example).

4.1 Passband Gain as a Function of N and k

This section provides mathematical basis for the observed gain in the filter's passband response. This analysis makes use of a free program called "Graph" which allows plotting of functions and data points.

Figure 43 shows the total response of an 8-stage filter (equation 24) as well as the individual stage responses. Plotting the response over normalized frequency, x, defined as the original frequency range divided by the center frequency, F_c, of the cascaded response re-centers the response around an x-axis value of 1 for the purpose of generalizing the investigation. This figure also defines the referencing convention for the center, or peak, frequency (f_n) corresponding to each individual stage and for the areas of interest referred to later as the "mid-band region" and the "edge region".

$$H(x) = 20\,log_{10}\left[\frac{\left|1+\frac{x}{k^3\sqrt{k}}\right|}{\sqrt{1+\left(\frac{x}{k^3\sqrt{k}}\right)^2}} \times \frac{\left|1+\frac{x}{k^2\sqrt{k}}\right|}{\sqrt{1+\left(\frac{x}{k^2\sqrt{k}}\right)^2}} \times \frac{\left|1+\frac{x}{k\sqrt{k}}\right|}{\sqrt{1+\left(\frac{x}{k\sqrt{k}}\right)^2}} \times \frac{\left|1+\frac{x}{\sqrt{k}}\right|}{\sqrt{1+\left(\frac{x}{\sqrt{k}}\right)^2}} \times \frac{\left|1+x\sqrt{k}\right|}{\sqrt{1+\left(x\sqrt{k}\right)^2}} \times \frac{\left|1+xk\sqrt{k}\right|}{\sqrt{1+\left(xk\sqrt{k}\right)^2}} \times \frac{\left|1+xk^2\sqrt{k}\right|}{\sqrt{1+\left(xk^2\sqrt{k}\right)^2}} \times \frac{\left|1+xk^3\sqrt{k}\right|}{\sqrt{1+\left(xk^3\sqrt{k}\right)^2}}\right] \quad (24)$$

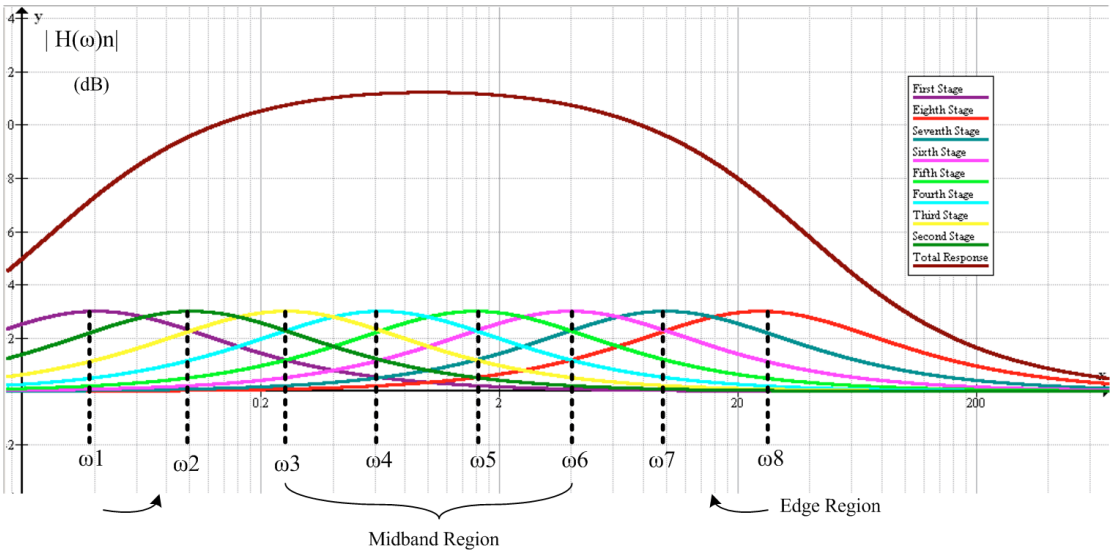

Figure 43. Transfer function plot for multiple stage, effective bandpass, filter

Each individual stage in the cascade provides a single peak at f_n, where n corresponds to the stage number. The numerical values of f_n are chosen equidistantly from each other on a logarithmic scale; this spacing produces nearly equi-ripple stopband characteristics (see Figure 39-Figure 42). Mathematically, this means:

$$\frac{f_2}{f_1} = \frac{f_3}{f_2} = \frac{f_n}{f_{n-1}} = k \quad (25)$$

where *k* corresponds to a number termed "frequency spacing", the ratio between the equidistant peak frequencies.

Realize that the center frequency, F_c, for a total response differs depending on even or odd filter order. For odd system filter order, the center frequency coincides with the central peak; for example, for an $N = 3$ filter with peaks at $f_1, f_2,$ and f_3 the

center frequency is f_2. For even system filter order, the center frequency falls between the two most central frequencies; for example an $N = 8$ filter, like the one shown in Figure 38, has an overall center frequency between f_4 and f_5. Visualize this in a pole-zero plot (Figure 44) where the dashed arc represents the overall center frequency.

Naming frequencies with respect to the overall center frequency proves useful in future design relationship derivations. Instead of f_n where n corresponds to stage number, the frequencies become f_{+m} or f_{-m} where m the relative position compared to F_c. For an $N = 3$ filter, f_1 becomes f_{-1}, f_2 becomes F_c, and f_3 becomes f_{+1}. The frequencies use the same k relationship determined before. With respect to the center frequency, f_{+m} and f_{-m} can relate by:

$$\frac{f_{-1}}{F_c} = \frac{1}{k},\ \frac{f_{+1}}{F_c} = k,\ \frac{f_{+2}}{F_c} = k^2,\ \frac{f_{\pm m}}{F_c} = k^{\pm m} \qquad (26)$$

However, for an even order filter, because the center frequency does not match up with an actual stage peak, F_c, the individual peak frequencies relate to the center differently. For an $N = 2$ filter, f_1 becomes f_{-1}, f_2 becomes f_{+1}, and F_c centers between the two:

$$\frac{f_{-1}}{F_c} = \frac{1}{\sqrt{k}},\ \frac{f_{+1}}{F_c} = \sqrt{k},\ \frac{f_{+2}}{F_c} = k^{3/2},\ \frac{f_{\pm m}}{F_c} = k^{\pm m/2} \qquad (27)$$

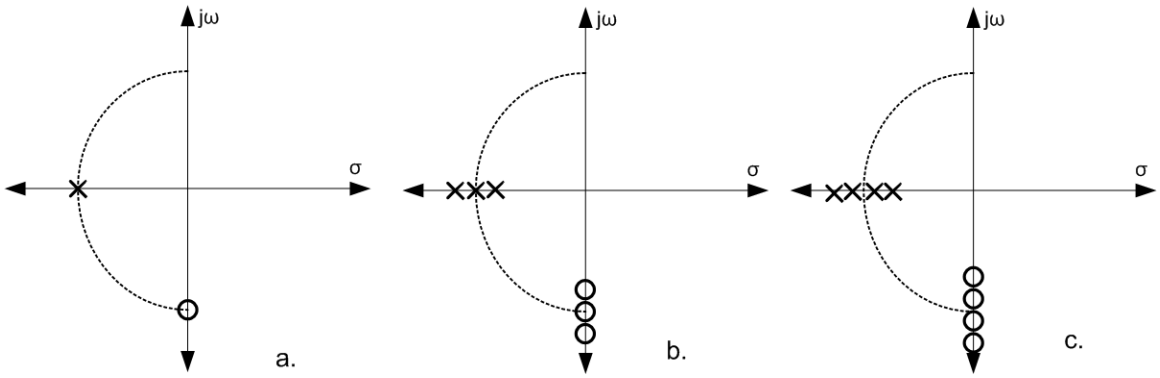

Figure 44. Determining system central frequency using pole-zero plots

Note that the numbering convention described above and used for the following discussions arbitrarily assigns consecutive frequency peak numbers to corresponding stage number, i.e. f_2 corresponds to the center frequency for the second stage. Assume this for referencing purposes; see [7] for a discussion on the topic of stage arrangement.

4.1.1 Even and Odd Orders

To determine a general equation for maximum mid-band gain, first examine the example normalized magnitude transfer functions, H_N where N represents system order, for different order filters (equations 27-32). First observe that odd-order filters (equations 27-29) express differently from even-order filters (equations 30-32) and therefore a different generalized equation becomes necessary for each case.

$$H_3(x) = 20\,log_{10}\left[\frac{\left|1+\frac{x}{k}\right|}{\sqrt{1+\left(\frac{x}{k}\right)^2}} \times \frac{|1+x|}{\sqrt{1+(x)^2}} \times \frac{|1+kx|}{\sqrt{1+(kx)^2}}\right] \quad (28)$$

$$H_5(x) = 20\,log_{10}\left[\frac{\left|1+\frac{x}{k^2}\right|}{\sqrt{1+\left(\frac{x}{k^2}\right)^2}} \times \frac{\left|1+\frac{x}{k}\right|}{\sqrt{1+\left(\frac{x}{k}\right)^2}} \times \frac{|1+x|}{\sqrt{1+(x)^2}} \times \frac{|1+kx|}{\sqrt{1+(kx)^2}} \times \frac{|1+k^2x|}{\sqrt{1+(k^2x)^2}}\right] \quad (29)$$

$$H_7(x) = 20\,log_{10}\left[\frac{\left|1+\frac{x}{k^3}\right|}{\sqrt{1+\left(\frac{x}{k^3}\right)^2}}\times\frac{\left|1+\frac{x}{k^2}\right|}{\sqrt{1+\left(\frac{x}{k^2}\right)^2}}\times\frac{\left|1+\frac{x}{k}\right|}{\sqrt{1+\left(\frac{x}{k}\right)^2}}\times\frac{|1+x|}{\sqrt{1+(x)^2}}\times\frac{|1+kx|}{\sqrt{1+(kx)^2}}\times\frac{|1+k^2x|}{\sqrt{1+(k^2x)^2}}\times\frac{|1+k^3x|}{\sqrt{1+(k^3x)^2}}\right] \quad (30)$$

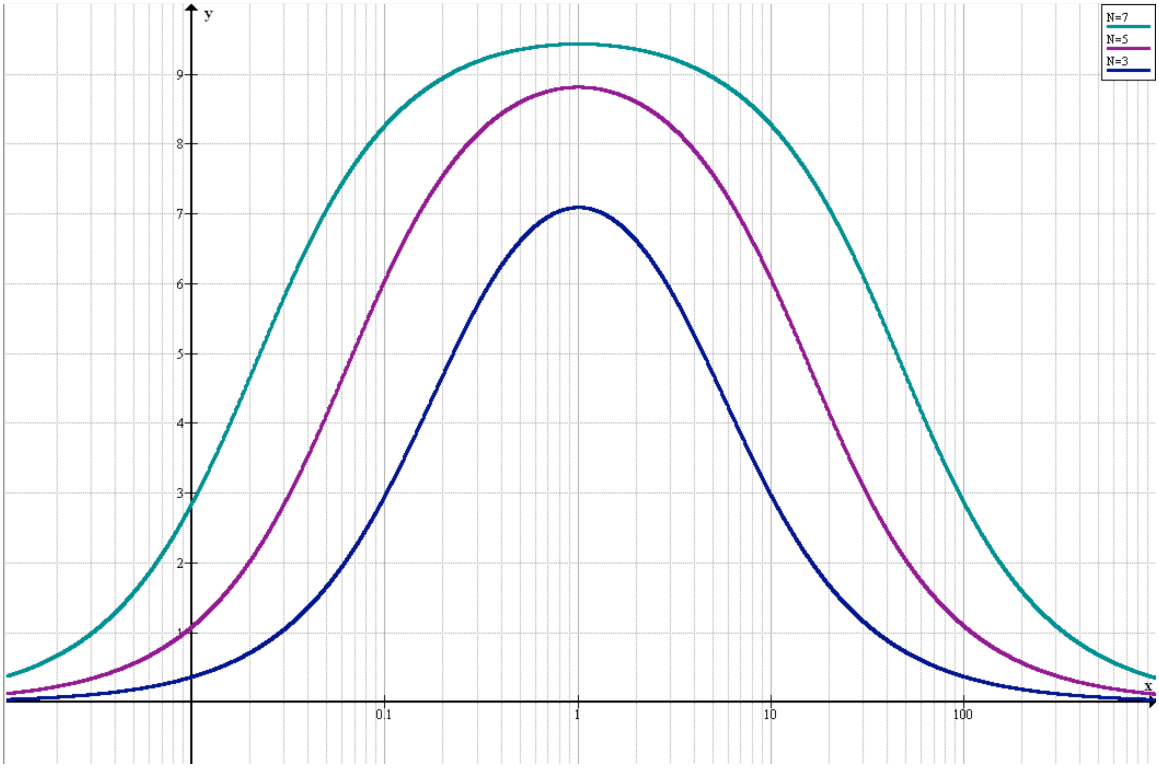

Figure 45. Pass-band plot for N=3, 5, 7 (normalized frequency, k = 1)

$$H_2(x) = 20\,log_{10}\left[\frac{\left|1+\frac{x}{\sqrt{k}}\right|}{\sqrt{1+\left(\frac{x}{\sqrt{k}}\right)^2}}\times\frac{|1+x\sqrt{k}|}{\sqrt{1+(x\sqrt{k})^2}}\right] \quad (31)$$

$$H_4(x) = 20\,log_{10}\left[\frac{\left|1+\frac{x}{k\sqrt{k}}\right|}{\sqrt{1+\left(\frac{x}{k\sqrt{k}}\right)^2}}\times\frac{\left|1+\frac{x}{\sqrt{k}}\right|}{\sqrt{1+\left(\frac{x}{\sqrt{k}}\right)^2}}\times\frac{|1+x\sqrt{k}|}{\sqrt{1+(x\sqrt{k})^2}}\times\frac{|1+xk\sqrt{k}|}{\sqrt{1+(xk\sqrt{k})^2}}\right] \quad (32)$$

$$H_6(x) = 20\,log_{10}\left[\frac{\left|1+\frac{x}{k^2\sqrt{k}}\right|}{\sqrt{1+\left(\frac{x}{k^2\sqrt{k}}\right)^2}}\times\frac{\left|1+\frac{x}{k\sqrt{k}}\right|}{\sqrt{1+\left(\frac{x}{k\sqrt{k}}\right)^2}}\times\frac{\left|1+\frac{x}{\sqrt{k}}\right|}{\sqrt{1+\left(\frac{x}{\sqrt{k}}\right)^2}}\times\frac{|1+x\sqrt{k}|}{\sqrt{1+(x\sqrt{k})^2}}\times\frac{|1+xk\sqrt{k}|}{\sqrt{1+(xk\sqrt{k})^2}}\times\frac{|1+xk^2\sqrt{k}|}{\sqrt{1+(xk^2\sqrt{k})^2}}\right] \quad (33)$$

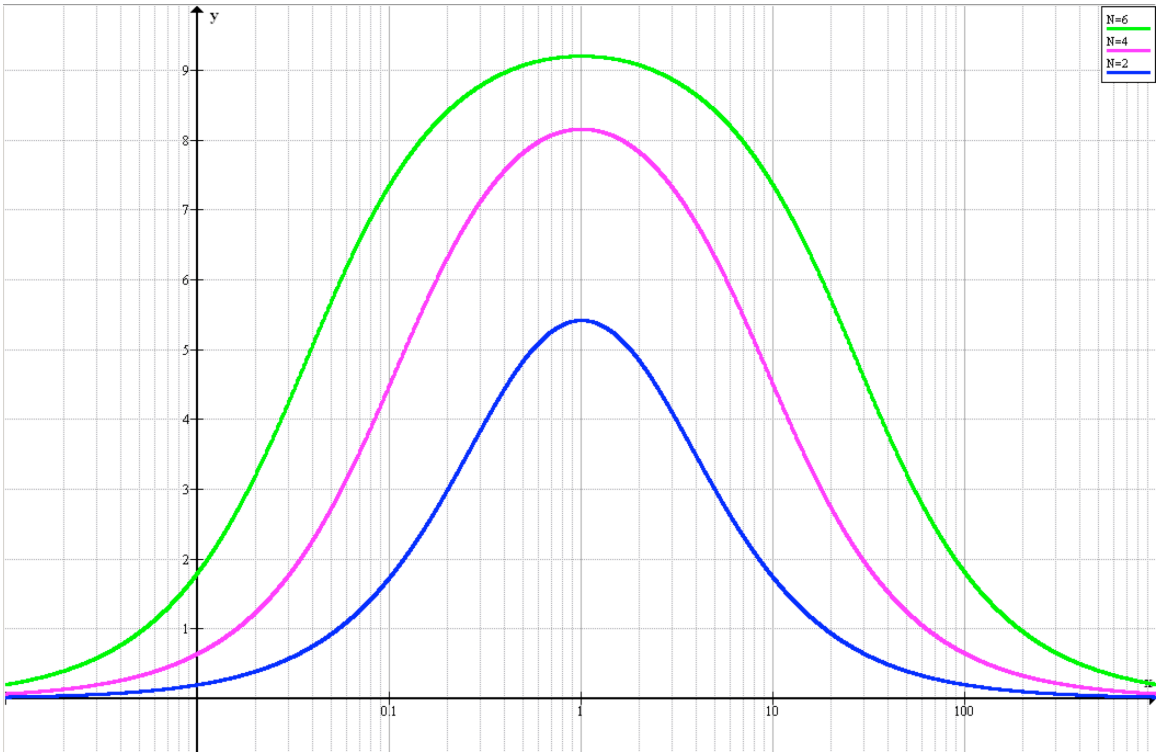

Figure 46. Pass-band plot for N=2, 4, 6 (normalized frequency, k = 1)

To find a closed-form expression for peak gain, examine the $N = 3$ case (Equation 29, shown again below).

$$H_3(x) = 20\log_{10}\left[\frac{\left|1+\frac{x}{k}\right|}{\sqrt{1+\left(\frac{x}{k}\right)^2}} \times \frac{|1+x|}{\sqrt{1+(x)^2}} \times \frac{|1+kx|}{\sqrt{1+(kx)^2}}\right]$$

Note that the first term within the log function corresponds to the lowest frequency, f_1, which corresponds also to f_{-1}. The second term corresponds to the center frequency, F_c, or f_2, and the third term corresponds the highest frequency, f_3 or f_{+1}. The peak gain occurs at the center frequency, F_c; in the normalized expression, this means x should equal 1.

$$H_3(x) = 20\,log_{10}\left[\frac{\left|1+\frac{1}{k}\right|}{\sqrt{1+\left(\frac{1}{k}\right)^2}} \times \frac{|1+1|}{\sqrt{1+(1)^2}} \times \frac{|1+k\cdot 1|}{\sqrt{1+(k\cdot 1)^2}}\right] = 20\,log_{10}\left[\frac{\left|1+\frac{1}{k}\right|}{\sqrt{1+\left(\frac{1}{k}\right)^2}} \times \frac{|2|}{\sqrt{2}} \times \frac{|1+k|}{\sqrt{1+(k)^2}}\right] = 20\,log_{10}\left[\frac{\frac{1}{k}|k+1|}{\frac{1}{k}\sqrt{(k)^2+1}} \times \sqrt{2} \times \frac{|1+k|}{\sqrt{1+(k)^2}}\right] \quad (34)$$

Factoring out $\frac{1}{\mathrm{k}}$ from the numerator and denominator of first term makes the first and third terms identical (the $\frac{1}{\mathrm{k}}$ factor cancels out) and the second term becomes a constant, independent of k. The first and last terms have the same contribution to peak gain. Because of the log function, multiplication becomes addition and the function simplifies:

$$H_3(x) = 20\,log_{10}\left[\sqrt{2}\right] + 20\,log_{10}\left[\frac{|k+1|}{\sqrt{(k)^2+1}}\right] + 20\,log_{10}\left[\frac{|1+k|}{\sqrt{1+(k)^2}}\right] = 3dB + 2\cdot 20\,log_{10}\left[\frac{|1+k|}{\sqrt{1+(k)^2}}\right] = 3dB + 40\,log_{10}\left[\frac{|1+k|}{\sqrt{1+(k)^2}}\right] \quad (35)$$

Realizing that this generalizes for any odd N because the contribution from additional stages branches out symmetrically about the central frequency:

$$Odd\ Peak\ Gain = 20\,log_{10}\sqrt{2} + 40\sum_{l=1}^{\frac{N-1}{2}} log_{10}\frac{k^l+1}{\sqrt{k^{2l}+1}} \quad (36)$$

Where *N* corresponds to the number of stages and *k* corresponds to frequency spacing.

The case for an even value of *N* is different again because of the individual peak frequencies relationship to the system center frequency, F_c. For the $N = 2$ case (Equation 32):

$$H_2(x) = 20\log_{10}\left[\frac{\left|1+\frac{x}{\sqrt{k}}\right|}{\sqrt{1+\left(\frac{x}{\sqrt{k}}\right)^2}} \times \frac{\left|1+x\sqrt{k}\right|}{\sqrt{1+\left(x\sqrt{k}\right)^2}}\right]$$

Again, setting the normalized frequency, x, to 1 to find the peak gain (see Figure 45):

$$H_2(x) = 20\,log_{10}\left[\frac{\left|1+\frac{1}{\sqrt{k}}\right|}{\sqrt{1+\left(\frac{1}{\sqrt{k}}\right)^2}} \times \frac{\left|1+1\cdot\sqrt{k}\right|}{\sqrt{1+\left(1\cdot\sqrt{k}\right)^2}}\right] = 20\,log_{10}\left[\frac{\left|1+\frac{1}{\sqrt{k}}\right|}{\sqrt{1+\left(\frac{1}{\sqrt{k}}\right)^2}} \times \frac{\left|1+\sqrt{k}\right|}{\sqrt{1+\left(\sqrt{k}\right)^2}}\right] =$$
$$20\,log_{10}\left[\frac{\frac{1}{\sqrt{k}}\left|\sqrt{k}+1\right|}{\frac{1}{\sqrt{k}}\sqrt{\left(\sqrt{k}\right)^2+1}} \times \frac{\left|1+\sqrt{k}\right|}{\sqrt{1+\left(\sqrt{k}\right)^2}}\right] \quad (37)$$

Similar to the $N = 3$ case, this time factoring out a value of $\frac{1}{\sqrt{k}}$ reveals that the first and second term equate. Again using the properties of log:

$$H_2(x) = 20\,log_{10}\left[\frac{\left|\sqrt{k}+1\right|}{\sqrt{\left(\sqrt{k}\right)^2+1}}\right] + 20\,log_{10}\left[\frac{\left|1+\sqrt{k}\right|}{\sqrt{1+\left(\sqrt{k}\right)^2}}\right] = 2\cdot 20\,log_{10}\left[\frac{\left|1+\sqrt{k}\right|}{\sqrt{1+\left(\sqrt{k}\right)^2}}\right] =$$
$$40\,log_{10}\left[\frac{\left|1+\sqrt{k}\right|}{\sqrt{1+\left(\sqrt{k}\right)^2}}\right] \quad (38)$$

From this, the equation can be expanded for a general even N case:

$$\textit{Even Peak Gain} = 40\sum_{l=1}^{\frac{N}{2}} log_{10}\frac{k^{l-\frac{1}{2}}+1}{\sqrt{k^{2l-1}+1}} \quad (39)$$

Where N corresponds to the number of stages and k corresponds to frequency spacing.

Table 10 validates the derived expressions. It contains the results of evaluating equations 37 and 40 with Matlab and simulating with ideal component values in LTspice.

Table 10. Matlab Values and LTspice Simulation

Stage	Mid-Band Gain (dB)	
	Matlab	**LTspice**
1	3.010	3.010
2	5.705	5.705
3	7.910	7.910
4	9.604	9.604
5	10.851	10.851

4.2 Passband 3dB Bandwidth as a Function of *N* and *k*

This section derives a mathematical expression for the 3dB bandwidth of the filter's passband response. While equations 37 and 40 provide closed-form expressions for peak gain as a function of the number of stages and the frequency spacing, there is no comparably simple way of deriving such an expression for the 3dB bandwidth. The following calculations depend on a method of curve fitting performed in Excel. Remember that because a complex filter's primary use requires its asymmetric frequency response, the passband bandwidth must compare to the stopband bandwidth for proper functionality. In other words, the passband should measure wide enough to pass the desired signal while the stop-band should correspondingly size to reject any image signals. Consider also that certain combinations of filter order and frequency spacing (k) can result in "bandwidth shrinkage". This problem commonly arises when a higher order filter combines with very close frequency spacing in an attempt to achieve higher stopband attenuation.

4.2.1 Calculation

First consider the unique case of a single stage (N=1) filter. Figure 47 shows the passband response of a single stage filter. Under the assumption that -3dB frequencies down from the maximum passband gain define the passband bandwidth, the single stage filter has theoretically infinite bandwidth.

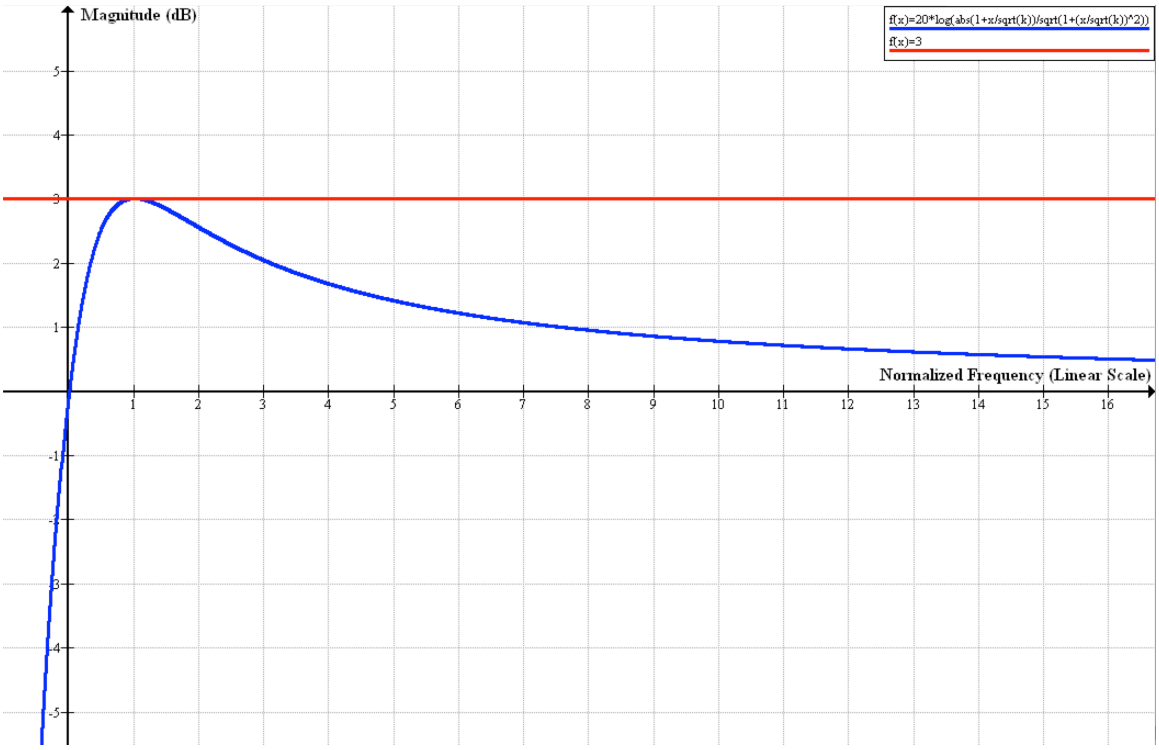

Figure 47. Passband response for single-stage, peak magnitude of 3dB, magnitude greater than 0dB for all positive frequency range

Next, consider the case of N larger than 1 and $k = 1$. With k set to 1, the individual stage notch frequencies are the same, visually, this look like Figure 48.

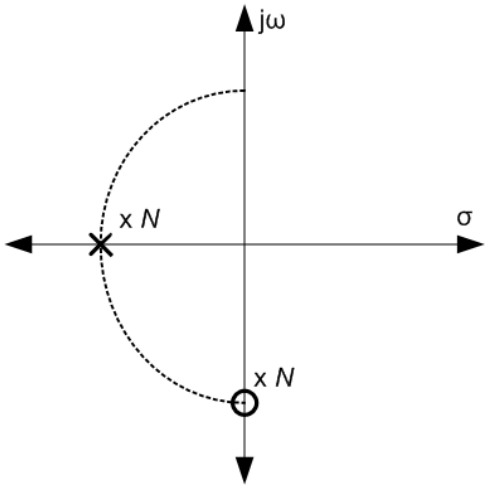

Figure 48. Pole-zero plot for k = 1

For N of 2 or larger, 3dB bandwidth is finite, unlike the $N = 1$ case. Figure 49 shows the measurements for normalized 3dB bandwidth versus N for $k = 1$ and N ranging from 2 to 15.

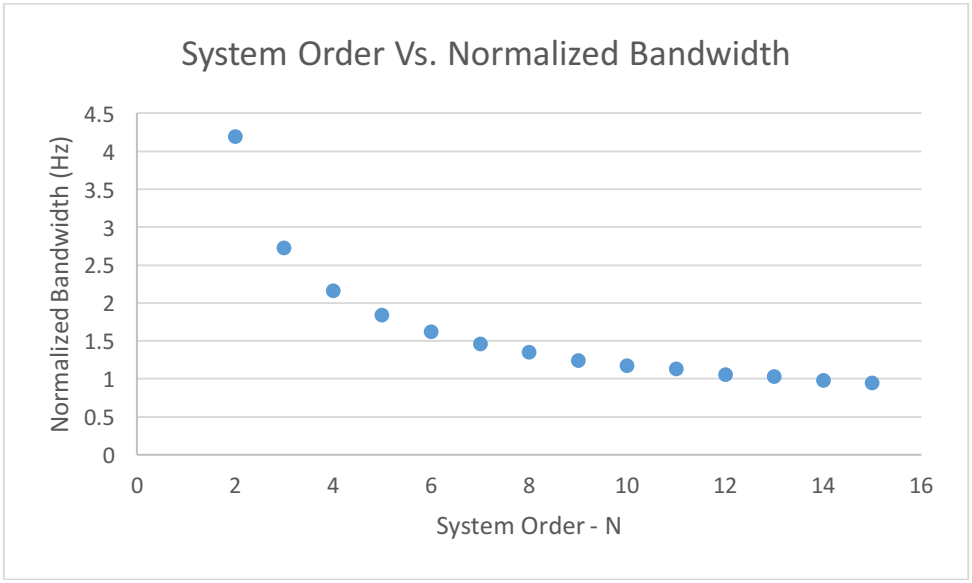

Figure 49. 3dB Normalized Bandwidth vs. N for k = 1, k=1 means identical stages

From this figure, curve fitting determines equation 40.

$$BW_{pass-k=1} = \frac{(0.85)}{(\sqrt[4]{N} - 1)} \qquad (40)$$

The next examination is of the relationship between frequency spacing, k, and the normalized system bandwidth. The figures below (Figure 50-Figure 56) graph this relationship over "reasonable" values of k [7] for $N = 2, 4, 6, 8, 3, 5, 7$. For each value of N, and exponential curve of the form below fits the points:

$$y = A \exp\left[\alpha \cdot x\right]$$

where A and α depend on N and x corresponds to k.

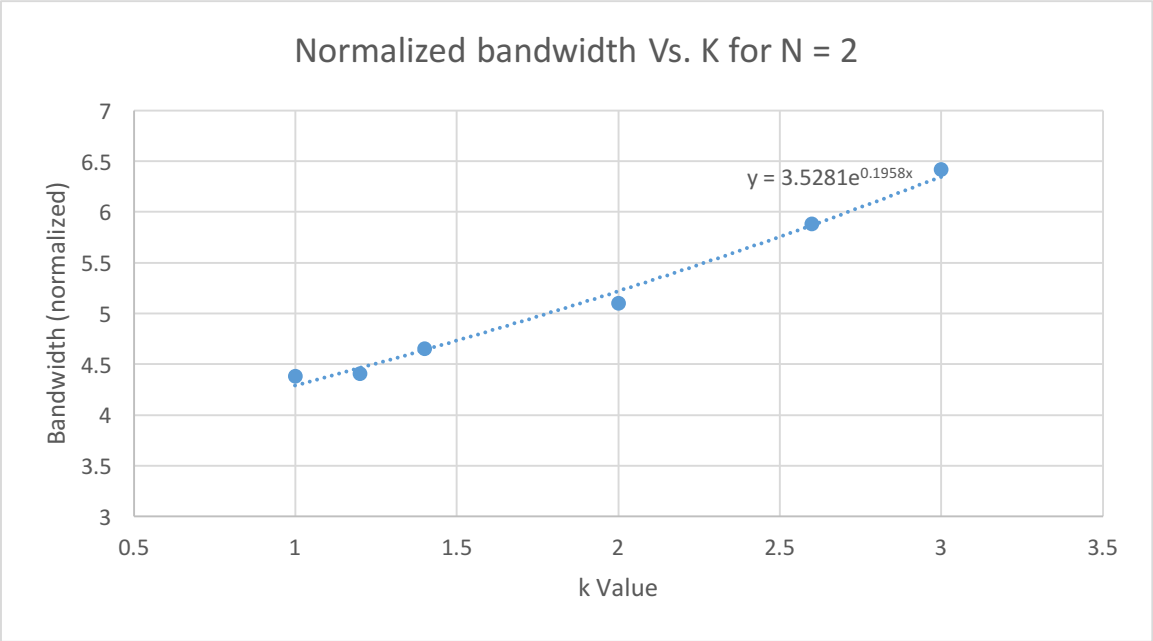

Figure 50. Normalized 3dB bandwidth for two stage topology vs. k

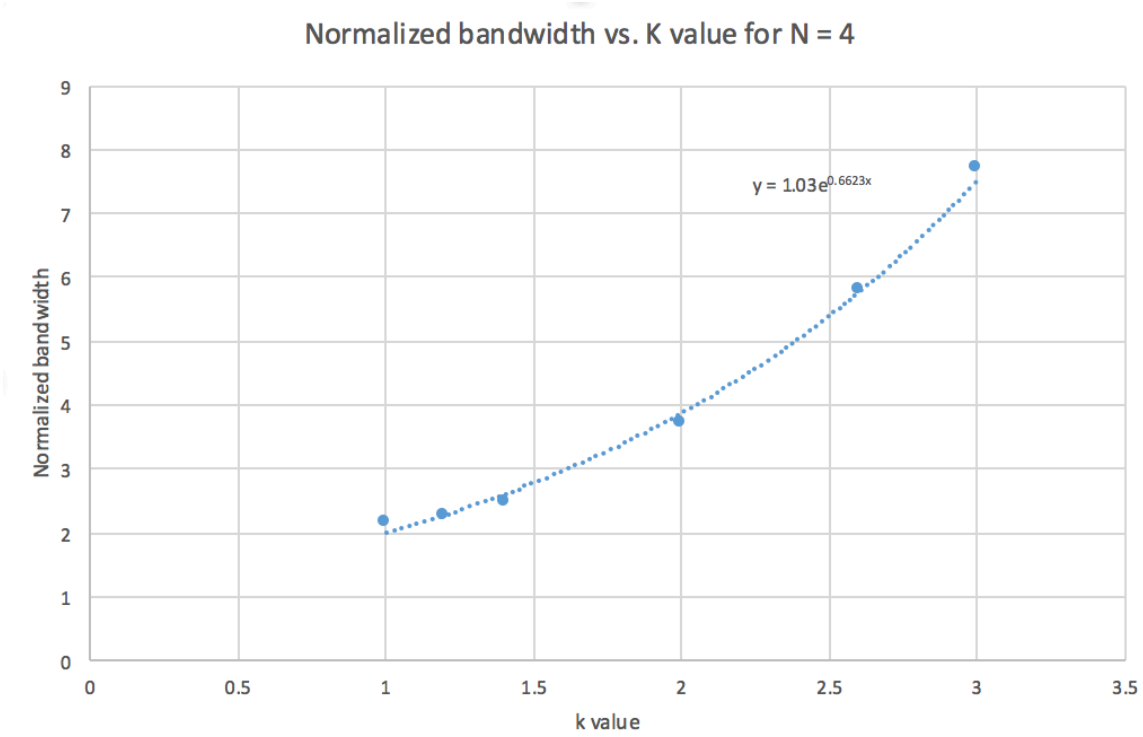

Figure 51. Normalized 3dB bandwidth for four stage topology vs. k

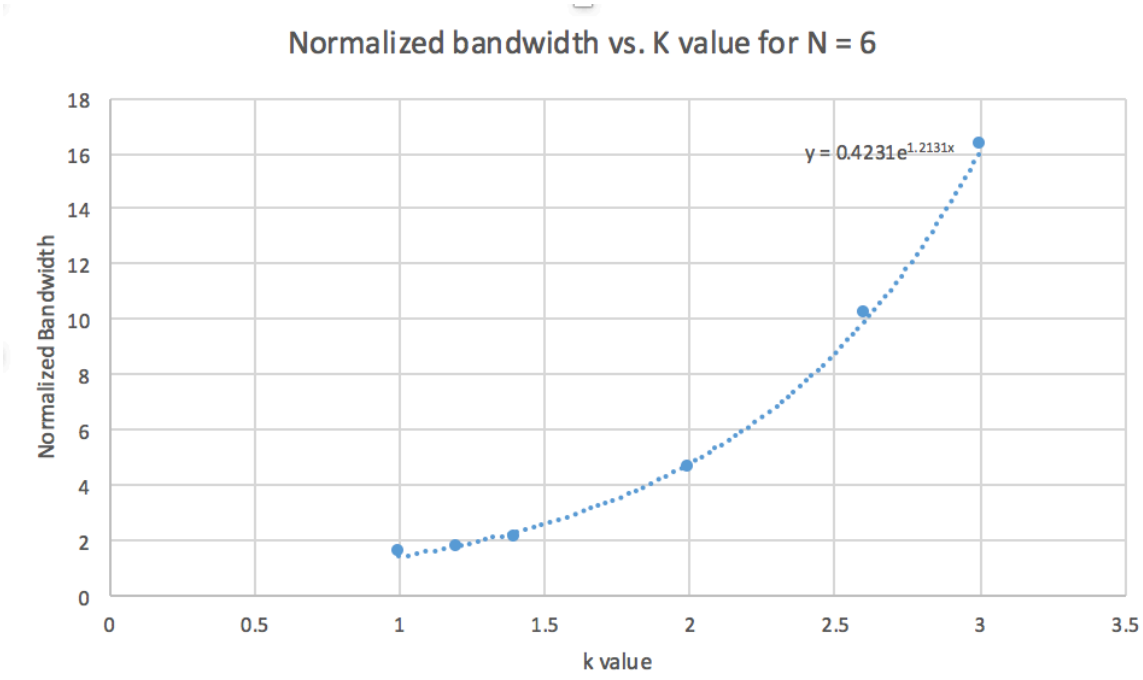

Figure 52. Normalized 3dB bandwidth for six stage topology vs. k

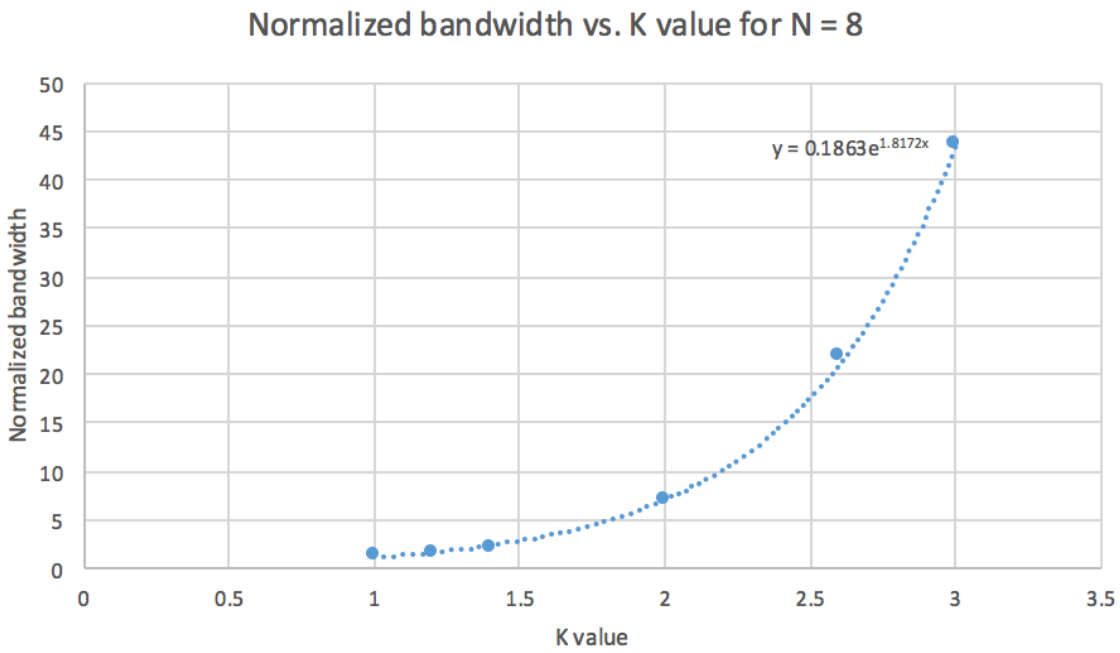

Figure 53. Normalized d3B bandwidth for eight stage topology vs. k

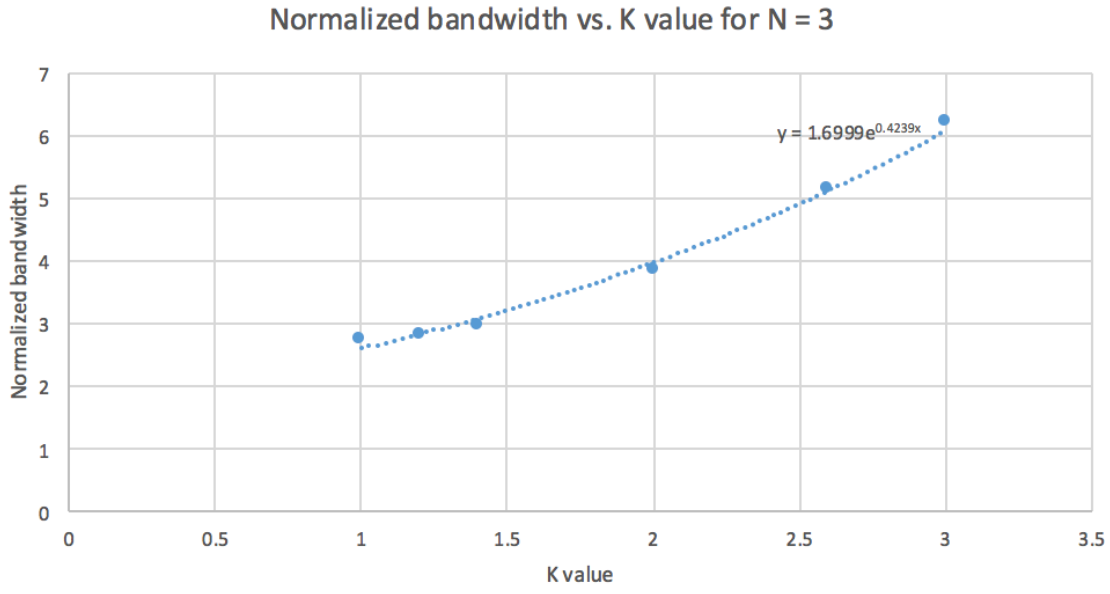

Figure 54. Normalized d3B bandwidth for three stage topology vs. k

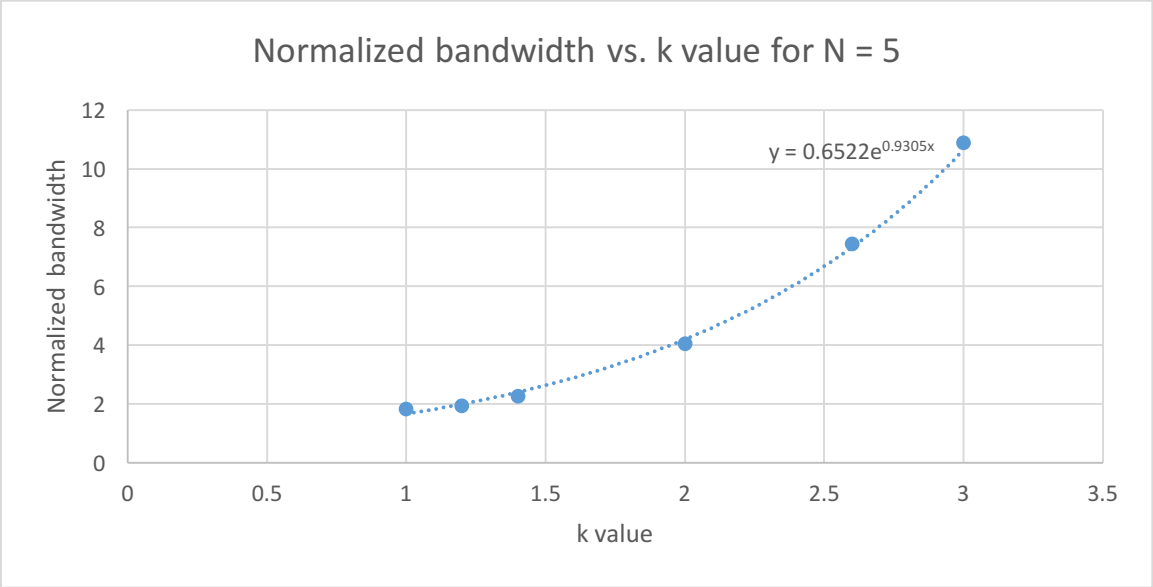

Figure 55. Normalized 3dB bandwidth for five stage topology vs. k

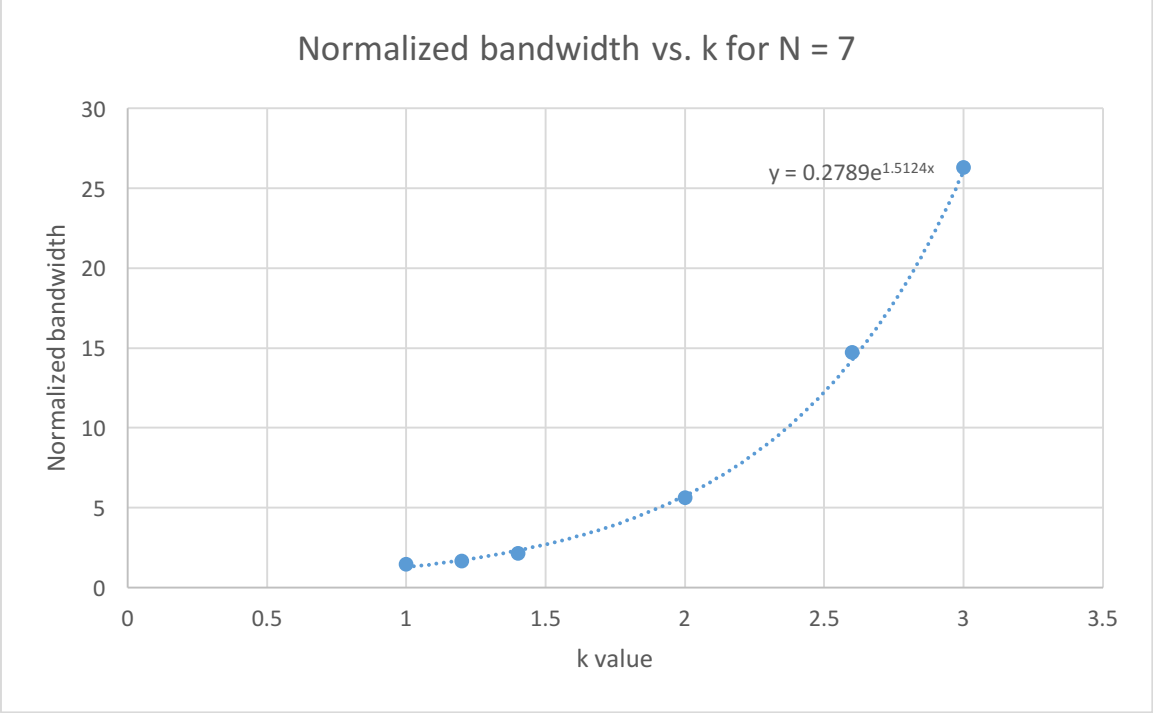

Figure 56. Normalized 3dB bandwidth for seven stage topology vs. k

From the figures above, all dependencies are fitted reasonably well using an exponential curve.

Building on equation (40) and using systematic trial and error determines the following equation for normalized bandwidth:

$$BW_{pass} = \frac{(0.85)}{(\sqrt[4]{N}-1)} * e^{\frac{(k-1)(N-1.3)}{4}} \quad (41)$$

Table 11 shows the accuracy of this equation. The largest difference between measured bandwidth and bandwidth calculated using equation (41) calculates to less than 11%. This equation also applies to the $k = 1$ case. For $k = 1$, the exponential term becomes unity and equation (41) equates to equation (40).

Table 11. Comparison of measured and calculated bandwidth

N	k	Measured	Calculated	% Difference
2	1	4.38	4.49	2.57
	1.2	4.41	4.65	5.50
	1.4	4.65	4.82	3.62
	2	5.1	5.35	4.93
	2.6	5.88	5.94	1.09
	3	6.42	6.38	-0.70
3	1	2.73	2.69	-1.49
	1.2	2.81	2.93	4.19
	1.4	2.97	3.19	7.33
	2	3.84	4.11	7.12
	2.6	5.13	5.31	3.47
	3	6.2	6.29	1.48
4	1	2.15	2.05	-4.55
	1.2	2.25	2.35	4.39
	1.4	2.47	2.69	8.83
	2	3.72	4.03	8.34
	2.6	5.79	6.04	4.36
	3	7.73	7.92	2.40
5	1	1.82	1.72	-5.72
	1.2	1.93	2.06	6.98
	1.4	2.25	2.48	10.4
	2	4.04	4.33	7.11
	2.6	7.438	7.54	1.35
	3	10.88	10.9	0.305

5. DESIGN WITH BANDWIDTH CONSTRAINT

Designing a filter focuses on choosing number of stages (*N*), and the notch frequency spacing (*k*), to meet given filter specifications. As discussed in Section 4, only two of the four quantities of interest may be enforced; the design is over-constraint.

To explore the effects of filter order on bandwidth, the following three designs demonstrate the process and performance of a 4-stage, 5-stage, and 6-stage filter.

For these design examples, the desired bandwidth corresponds to the approximate most sensitive range of human hearing (Figure 57), 400Hz to 15kHz. This frequency range encompasses the bandwidth used for telephony communications, 400Hz to 3.5kHz. The corner frequencies determine the central frequency of the whole filter (Equation 41).

$$f_c = \sqrt{f_1 * f_2} = \sqrt{15000 * 400} = 2449.5\ Hz \qquad (42)$$

Thus, the filter has a central frequency of 2.449kHz. The normalized bandwidth, found by dividing the bandwidth by the central frequency, becomes 5.96.

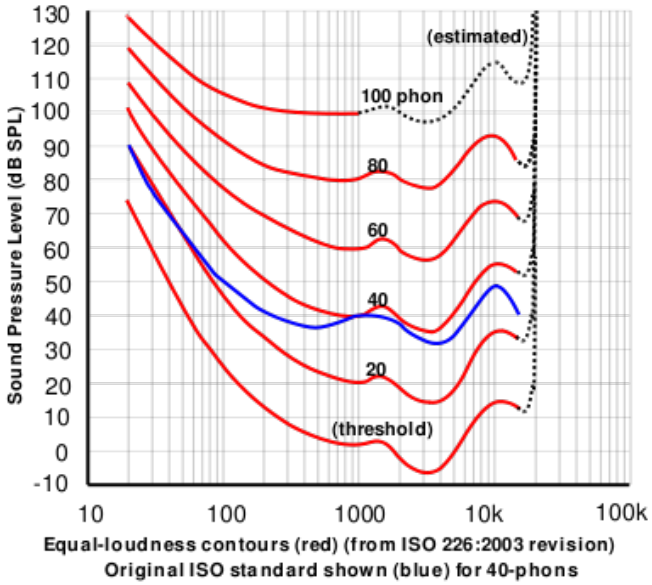

Figure 57. Human Ear Sensitivity [27]

With bandwidth determined, rearranging the equation for passband bandwidth (equation 41) yields the frequency spacing parameter k.

$$k = ln\left(\frac{BWpass*\left(\sqrt[4]{N}-1\right)}{0.085}\right) * \frac{4}{N-1.3} + 1 \qquad (43)$$

Each of the design examples below uses equation (43) to determine corresponding k for the three values of N.

N=4 Design:

Choosing a 4-stage parameter,

$$k = \frac{4}{4-1.3} * ln\left(\frac{5.96*\left(\sqrt[4]{4}-1\right)}{0.85}\right) + 1 = 2.579 \quad (44)$$

$$EdgeAtten = 84.13 * 2.579^{-1.344} = 23.54\ dB \quad (45)$$

$$Pass-band\ Gain\ (even) = 40\sum_{l=1}^{\frac{N}{2}} log_{10}\frac{k^{l-\frac{1}{2}}+1}{\sqrt{k^{2l-1}+1}} = 40\sum_{l=1}^{\frac{4}{2}} log_{10}\frac{2.579^{l-\frac{1}{2}}+1}{\sqrt{2.579^{2l-1}+1}} = 8.828\ dB \quad (46)$$

Note that because this is an even order filter, no individual center frequency equates to the overall filter central frequency. The individual frequencies derive from the relationship expressed in (27). The components chosen in Table 12 come from the general equation for the RC time constant.

Table 12. Component values for N=4 design

Stage	Stage Center Frequency (Hz)	Component Values	
		Standard 1% Capacitor (nF)	Standard 1% Resistor (kΩ)
1	3.934k	1	40.2/80.6/20k
2	10.15k	1	15.8/31.6k/7.87
3	1.525k	3.3	31.6/63.4/15.8
4	591.12	3.3	26.7/53.4/13.3

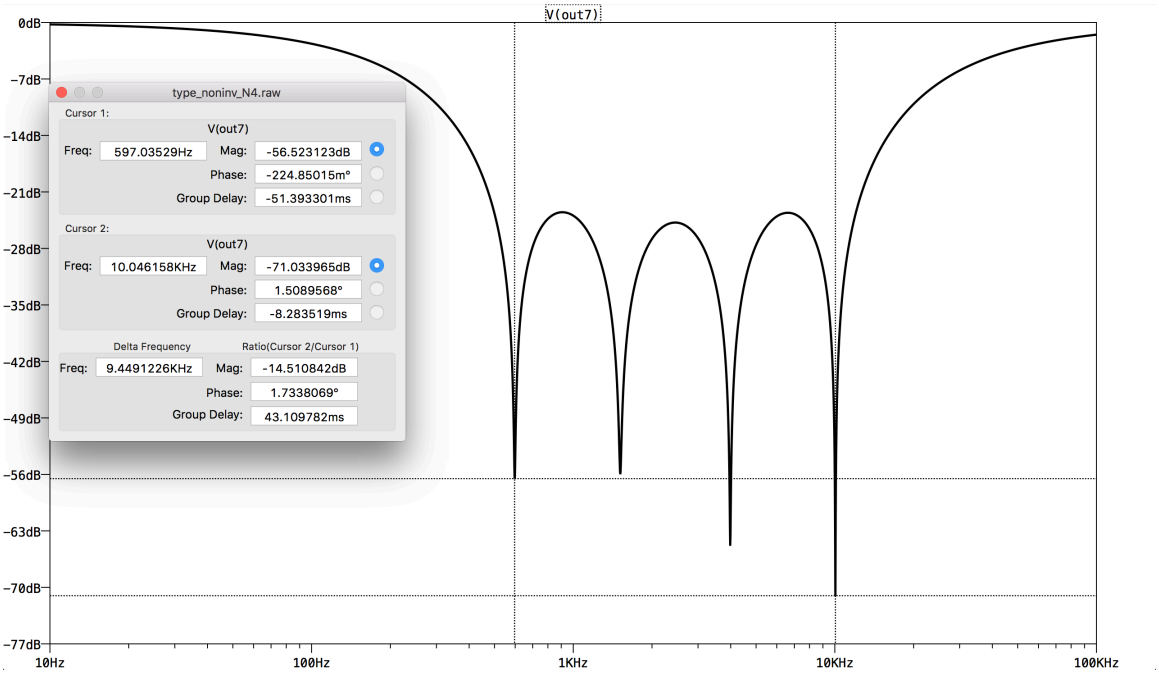

Figure 58. Stopband for N=4 design

Stop-band Bandwidth: 9.45kHz

Stop-band Attenuation: 23.5dB

Note that stop-band bandwidth measures from the first stop-band notch to the last stop-band notch (refer to [7] for reasoning), as such, this is a conservative estimate of stop-band bandwidth.

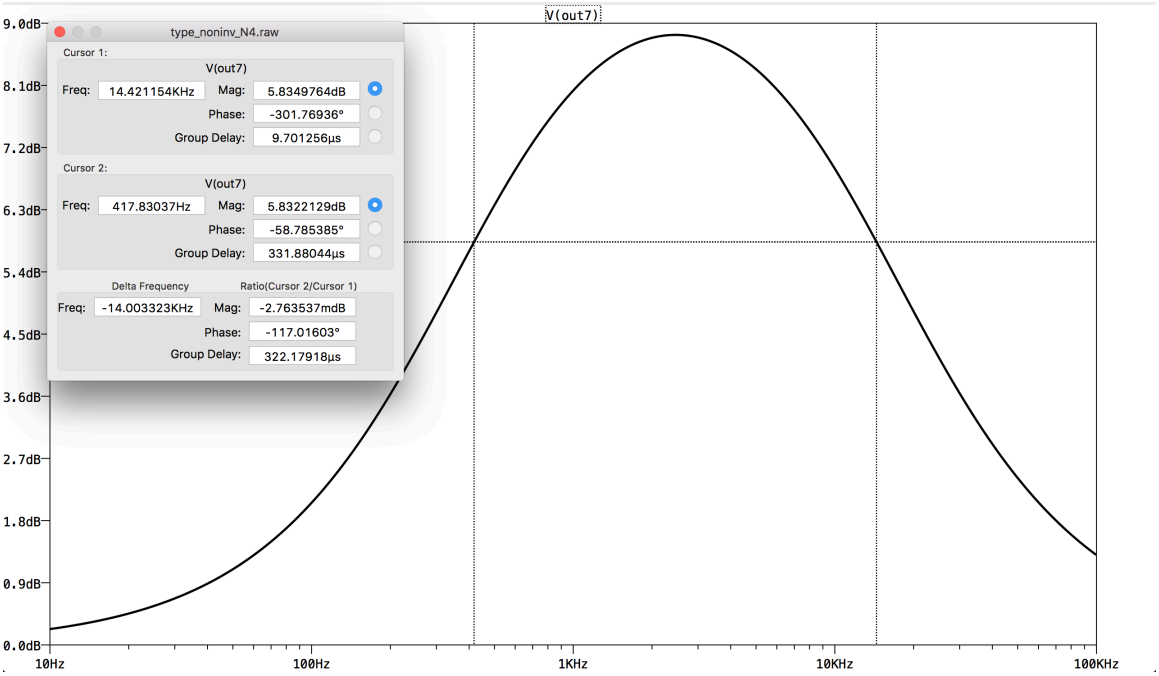

Figure 59. Passband for N=4 design

Pass-band Bandwidth: 14.0 kHz

Passband Gain: 8.83dB

N=5 Design:

$$k = \frac{4}{5-1.3} * ln\left(\frac{4.86*\left(\sqrt[4]{5}-1\right)}{0.85}\right) + 1 = 2.346 \quad (47)$$

$$Pass-band\ gain\ (odd) = 20\,log_{10}\sqrt{2} + 40\sum_{l=1}^{\frac{N-1}{2}} log_{10}\frac{k^l+1}{\sqrt{k^{2l}+1}} = 20\,log_{10}\sqrt{2} + 40\sum_{l=1}^{\frac{5-1}{2}} log_{10}\frac{2.346^l+1}{\sqrt{2.346^{2l}+1}} = 10.346\,dB \quad (48)$$

Table 13. Component values for N=5

Stage	Stage Center Frequency (Hz)	Component Values	
		Standard 1% Capacitor (nF)	Standard 1% Resistor (kΩ)
1	2.448k	1	64.9/130/32.4
2	5.746k	1	28/56.2/14
3	13.482k	1	11.8/23.7/5.9
4	1.044k	10	15/30.1/7.5
5	445	10	35.7/71.5/17.8

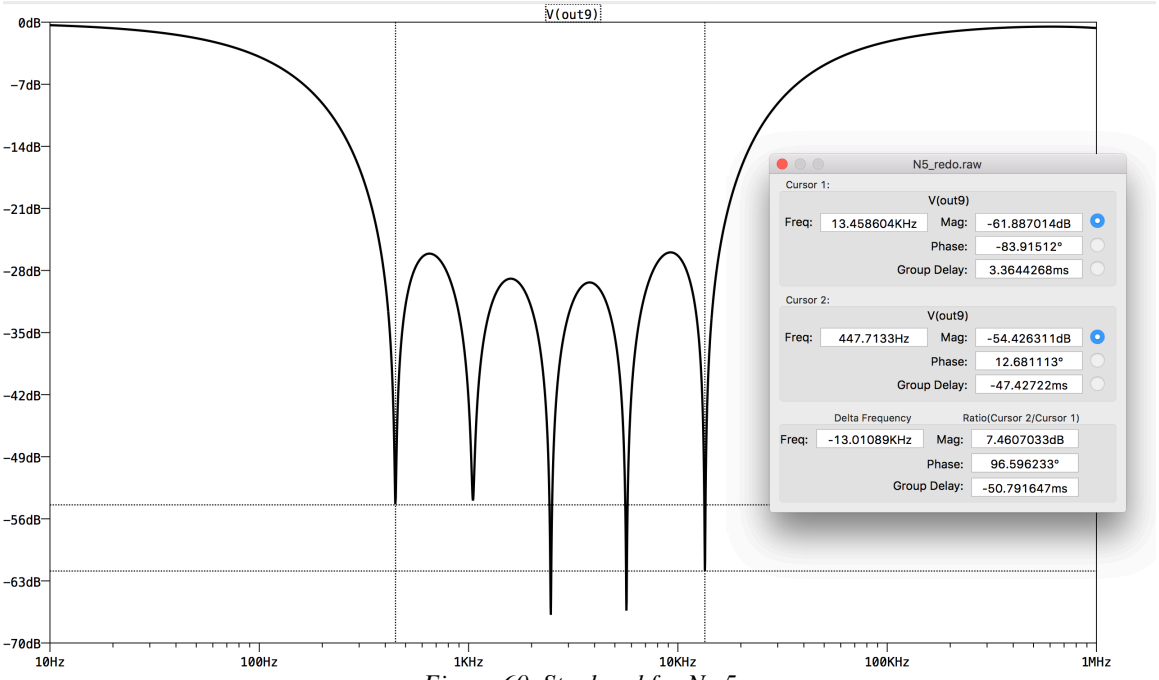

Figure 60. Stopband for N=5

Attenuation bandwidth: 13.01 kHz

Attenuation "floor": 26.1 dB

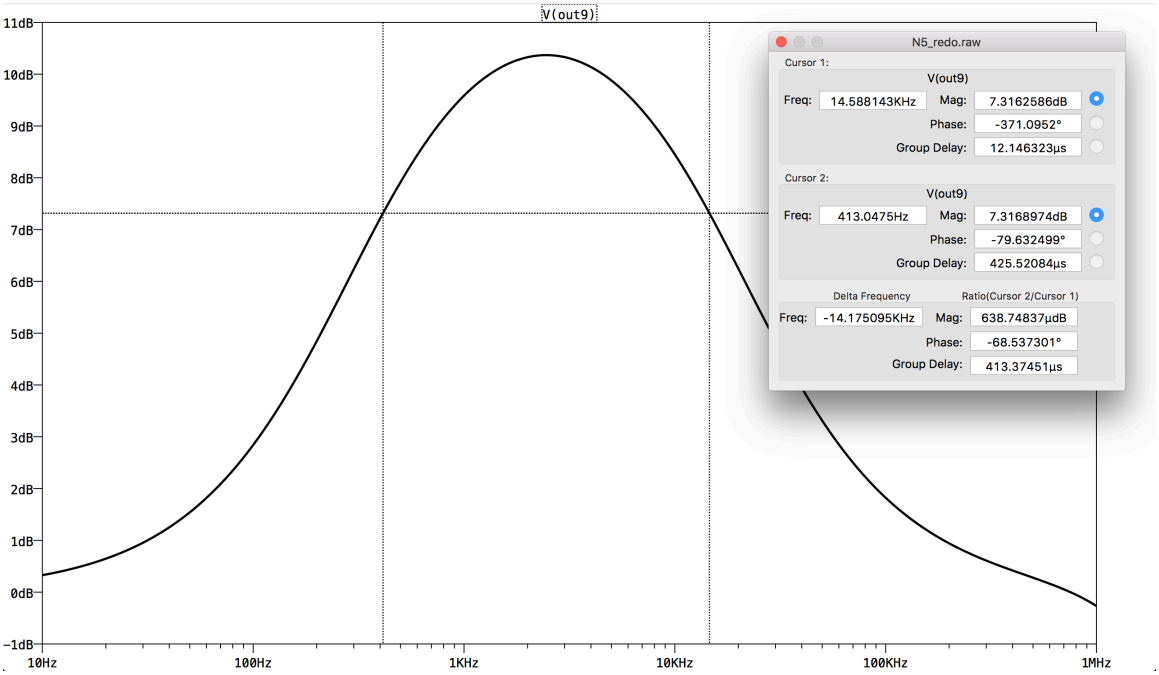

Figure 61. Passband for N=5

Band-pass bandwidth: 14.175 kHz

Band-pass gain: 10.36 dB

N=6 Design:

$$k = \frac{4}{6-1.3} * ln\left(\frac{4.86*\left(\sqrt[4]{6}-1\right)}{0.85}\right) + 1 = 2.17 \quad (49)$$

$$EdgeAtten = 84.13 * 2.17^{-1.344} = 29.66\ dB \quad (50)$$

$$Pass-band\ Gain\ (even) = 40\sum_{l=1}^{\frac{N}{2}} log_{10}\frac{k^{l-\frac{1}{2}}+1}{\sqrt{k^{2l-1}+1}} = 40\sum_{l=1}^{\frac{6}{2}} log_{10}\frac{2.17^{l-\frac{1}{2}}+1}{\sqrt{2.17^{2l-1}+1}} = 11.786\ dB \quad (51)$$

Table 14. Component values for N=6

Stage	Stage Center Frequency (Hz)	Component Values	
		Standard 1% Capacitor (nF)	Standard 1% Resistor (kΩ)
1	3.609k	1	44.2/88.7/22.1
2	7.839	1	20.5/41.2/10.2
3	17.026k	1	9.31/18.7/4.64
4	1.662k	3.3	29.4/59/14.7
5	765.3	3.3	63.4/127/31.6
6	352.386	10	45.2/90.9/22.6

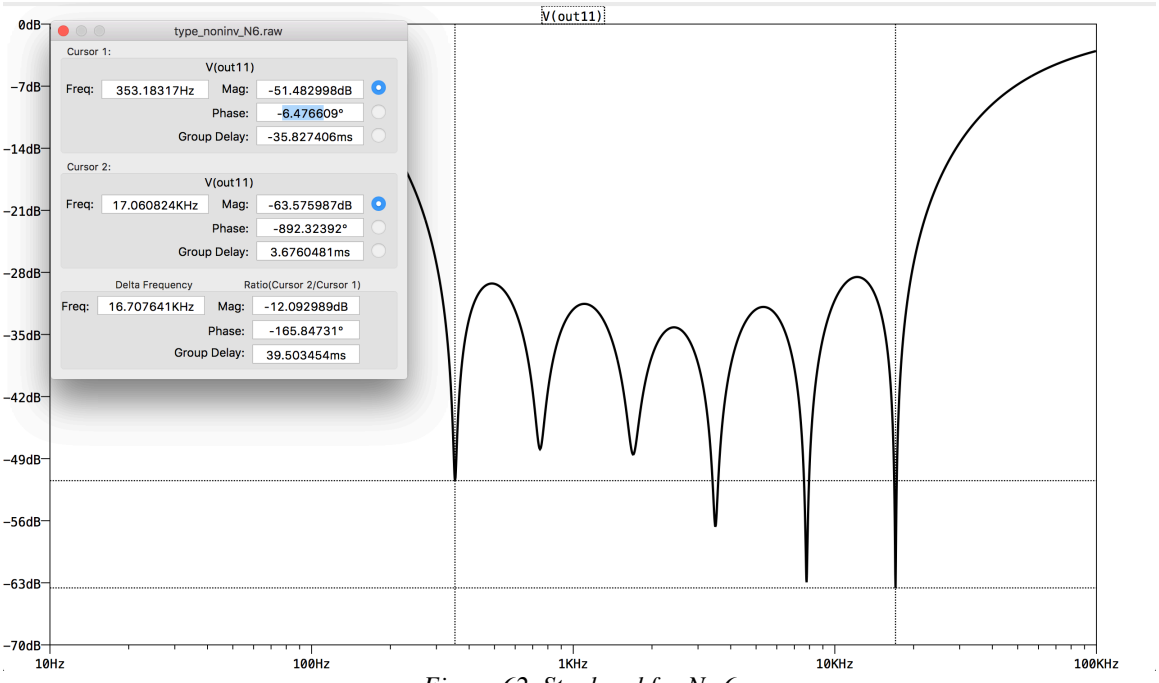

Figure 62. Stopband for N=6

Stop-band bandwidth: 16.7kHz

Stop-band attenuation: 28.5 dB

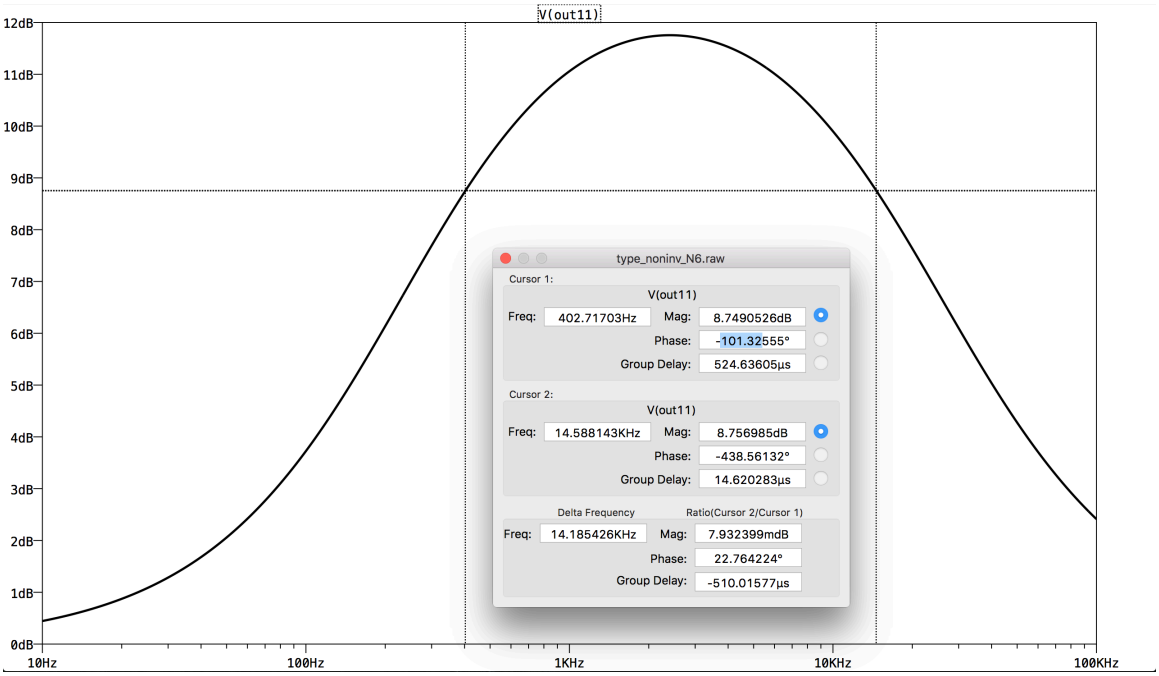

Figure 63. Passband for N=6

Pass-band bandwidth: 14.18 kHz

Pass-band gain: 11.75 dB

Table 15. Comparison of bandwidth measurements

N	Stop-band Bandwidth	Pass-Band Bandwidth
4	9.45kHz	14.0 kHz
5	13.01 kHz	14.175 kHz
6	16.7kHz	14.18 kHz

For a 4-stage implementation, the conservative stop-band bandwidth becomes smaller than the pass-band bandwidth, suggesting that the filter is unable to stop all the unwanted frequencies. In the 6-stage implementation, the stop-band bandwidth becomes larger than the pass-band bandwidth. The closest match between stop-band and pass-band bandwidths occurs with the 5-stage filter.

6. APPLICATIONS

In addition to the common applications discussed in Chapter 2 including quadrature generation for single sideband transmission and implementation of the Hilbert Transform and image rejection signal processing, this type of filter may find use in several less conventional applications.

Because this filter performs phase splitting, the output signals have the property of being 90° out of phase. Hartmann investigates the psychoacoustical effects associated with the perception of that phase shift, suggesting that phase splitting generates a pseudo-stereo type signal [28].

As mentioned in Chapter 2, networks with the ability to implement the Hilbert Transform find application in the realm of biosignal processing [21].

In addition, the closed-circle patterns that phase-split signals exhibit when viewed in X-Y mode on an oscilloscope present a new form of analyzing signals visually. This could have applications in detecting signal discontinuities or in finding a way for visual recognition of audio signals. One study on human ability to process complex images suggests that this type of visual recognition could become worthy of further study [29].

BIBLIOGRAPHY

[1] K. W. Martin, “Complex signal processing is not complex,” *IEEE Transactions on Circuits and Systems*, *vol. 51, no. 9, 2004*.

[2] Y. Jiao, Z. Huang, and L. Li, “CMOS analog polyphase filters for use in bluetooth systems,” *IEEE, 2008*.

[3] V. Prodanov, G. Palaskas, J. Glas, and V. Boccuzzi, “A CMOS AGC-less IF strip for bluetooth”.

[4] M. J. Gingell, “Single sideband modulation using sequence asymmetric polyphase networks,” *Electrical Commun.*, *vol. 48, no. 1 and 2, 1973*.

[5] F. Behbahani, Y. Kishigami, J. Leete, and A. A. Abidi, “CMOS mixers and polyphase filters for large image rejection,” *IEEE Journal of Solid State Circuits*, *vol. 36, no. 6, 2001*.

[6] J. Kaukovuori, K. Stadius, J. Ryynanen, and K. A. I. Halonen, “Analysis and design of passive polyphase filters,” *IEEE Transactions on Circuits and Systems*, *vol. 51, no. 10, 2008*.

[7] S. R. Johnston, “Complex Filters as Cascade of Buffered Gingell Structures: Design from Stop-Band Constraints.” California Polytechnic State University, San Luis Obispo, CA, 2016.

[8] R. Jaeger and T. Blalock, *Microelectronic circuit design*. New York: McGraw-Hill, 2011.

[9] K. Martin, "Complex Signal Processing is Not Complex," *IEEE TRANSACTIONS ON CIRCUITS AND SYSTEMS*, vol. 51, no. 9, pp. 1823-1836, 2004.

[10] A. Ambardar, *Analog and digital signal processing*. Pacific Grove, CA: Brooks/Cole Pub. Co., 1999.

[11] L. Z. W. R. a. O. F. Fayrouz Haddad, Mobile and Wireless Communications Network Layer and Circuit Level Design, Rijeka: INTECH, 2010.

[12] V. L. Larrowe, "Band-Pass Quadrature Filters," in *IEEE Transactions on Electronic Computers*, vol. EC-15, no. 5, pp. 726-731, Oct. 1966. doi: 10.1109/PGEC.1966.264560.
URL: http://ieeexplore.ieee.org/stamp/stamp.jsp?tp=&arnumber=4038878&isnumber=4038871

[13] S. Darlington, "Realization of a constant phase difference," in *The Bell System Technical Journal*, vol. 29, no. 1, pp. 94-104, Jan. 1950. doi: 10.1002/j.1538-7305.1950.tb00934.x.
URL: http://ieeexplore.ieee.org/stamp/stamp.jsp?tp=&arnumber=6769430&isnumber=6769427

[14] W. Saraga, "The Design of Wide-Band Phase Splitting Networks," in *Proceedings of the IRE*, vol. 38, no. 7, pp. 754-770, July 1950. doi: 10.1109/JRPROC.1950.233434.
URL: http://ieeexplore.ieee.org/stamp/stamp.jsp?tp=&arnumber=1701315&isnumber=35839

[15] H. T. Howard and A. M. Faries. "A constant phase-difference network and its application to a filter for an amateur-type transmitter," Department of Electrical Engineering of Leland Stanford Junior University, June 1955.

[16] P. Kiss, V. Prodanov and J. Glas, "Complex low-pass filters," *Circuits and Systems, 2002. ISCAS 2002. IEEE International Symposium on,* 2002, pp. I-525-I-528 vol.1. doi:10.1109/ISCAS.2002.1009893.
URL: http://ieeexplore.ieee.org/stamp/stamp.jsp?tp=&arnumber=1009893&isnumber=21766

[17] M. Feldman. "Hilbert transform in vibration analysis," *Mechanical Systems and Signal Processing,* Vol. 25, pp. 732-802, 2011.

[18] M. Johansson. "The Hilber Transform," Appied Mathematics, Vaxjo Univeristy.

[19] Yi-Wen Liu (2012). Hilbert Transform and Applications, Fourier Transform Applications, Dr Salih Salih (Ed.), ISBN: 978-953-51-0518-3, InTech, URL: http://www.intechopen.com/books/fourier-transform- applications/hilbert-transform-and-applications

[20] Hsu, Sheu and Hsue. "Overcoming the negative frequencies – instantaneous frequency and amplitude estimation using osculating circle method," *Journal of Marine Science and Technology*, Vol 19, No. 5, pp. 514-521, 2011.

[21] W. J. Freeman. "Hilbert transform for brain waves," July 2013.

[22] S. Bedrosian, "Normalized Design of 90° Phase-Difference Networks," in *IRE Transactions on Circuit Theory*, vol. 7, no. 2, pp. 128-136, Jun 1960. doi: 10.1109/TCT.1960.1086659,
URL: http://ieeexplore.ieee.org/stamp/stamp.jsp?tp=&arnumber=1086659&isnumber=23615

[23] W. Wieback. "Desig and Analysis of 90-Degree Phase Difference Networks," Harry Diamond Laboratories, May 1973.

[24] B. Hutchins. “The design of wideband analog 90° phase differencing networks without a large spread of capacitor values.”

[25] E. Stikvoort, "Polyphase Filter Section With OPAMPs," *IEEE TRANSACTIONS ON CIRCUITS AND SYSTEMS—II: ANALOG AND DIGITAL SIGNAL PROCESSING*, vol. 50, no. 6, pp. 376-378, 2003.

[26] I. Poole. “Resistor E Series: E3, E6, E12, E24, E48, E96 Values,” Radio-Electronics.com. URL: http://www.radio-electronics.com/info/data/resistor/e-series-e3-e6-e12-e24-e48-e96.php

[27] ISO226:2003. “Acoustics -- Normal equal-loudness-level contours,” Stage: 90.93 (2008-12-22), *International Organization fo r Standardization,* Standard, Geneva, Switzerland. (2008).

[28] W. M. Hartmann. “Some psychoacoustical experiments with all-pass networks,” *Am. J. Phys*., Vol. 47, No. 1, January 1979.

[29] S. Thorpe, D. Fize and C. Marlot. “Speed of processing in the human visual system,” in *Letters to Nature*, vol. 381, June 1996.

APPENDIX

Derivation of Equation 20:

For V_2 grounded:

$$\frac{-V_1}{R} + \frac{-V_{OUT}}{\frac{R}{s*C}} = 0$$

$$\frac{-V_1}{R} + \frac{-V_{OUT}}{R + \frac{1}{s*C}} = 0$$

$$\frac{-V_1}{R} + \frac{-V_{OUT}}{\frac{s*C}{s*C*R+1}} = 0$$

$$\frac{-V_1}{R} + \frac{-V_{OUT}}{\frac{R}{s*C*R+1}} = 0$$

$$\frac{-V_1}{R} = \frac{V_{OUT}}{\frac{R}{s*C*R+1}}$$

$$-V_1 \frac{1}{s*C*R+1} = V_{OUT}$$

$$H_1 = \frac{V_{OUT}}{V_1} = \frac{-1}{1+s*C*R}$$

For V_1 grounded:

$$\frac{V_+ - V_2}{\frac{1}{s*C}} + \frac{V_+ - 0}{\frac{R}{2}} = 0$$

$$\frac{V_- - 0}{R} + \frac{V_- - V_{OUT2}}{\frac{R}{s*C}} = 0$$

$$\frac{V_- - V_{OUT2}}{R + \frac{1}{s*C}}$$

$$V_+ = V_-$$

$$V_+ * s * C - V_2 * s * C + \frac{V_+ * 2}{R} = 0$$

$$V_+ \left(s*C + \frac{2}{R}\right) = V_2 * s * C$$

$$V_+ = V_2 * s * C$$

$$V_+ = V_2 * \frac{s*C}{s*C + \frac{2}{R}}$$

$$\frac{V_-}{R} + \frac{V_- - V_{OUT2}}{\frac{R}{s*C}} = 0$$

$$\frac{V_- - V_{OUT2}}{\frac{R*s*C+1}{s*C}}$$

$$\frac{V_-}{R} + \frac{V_- - V_{OUT2}}{\frac{R}{s*C*R+1}} = 0$$

$$\frac{V_R}{R} + \frac{V_-(s*C*R+1) - V_{OUT2}(s*C*R+1)}{R} = 0$$

$$V_- + V_-(s*C*R+1) - V_{OUT2}(s*C*R+1) = 0$$

$$V_-(1 + s*C*R + 1) = V_{OUT2}(s*C*R+1)$$

$$V_2 * \frac{s*C}{s*C+\frac{2}{R}}(1+s*C*R+1) = V_{OUT2}(s*C*R+1)$$

$$H_2 = \frac{V_{OUT2}}{V_2} = \frac{\frac{s*C(s*C*R+2)*R}{\left(s*C+\frac{2}{R}\right)*R}}{s*C*R} = \frac{s*C*R}{s*C*R+1}$$

V_{OUT}:

$$V_{OUT} = \frac{-1}{1+s*C*R} * V_1(s) + \frac{s*C*R}{1+s*C*R} * V_2(s)$$

Showing Response of Gingell Network to Positive and Negative Sequences:

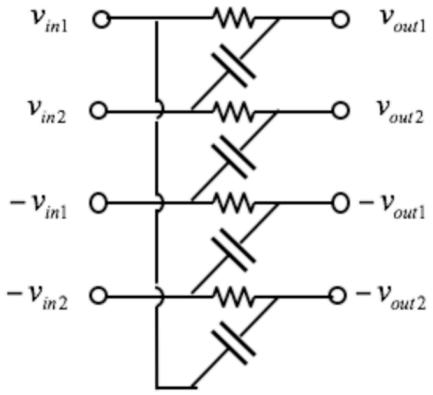

The transfer function can be described using superposition as:

$$V_{out1} = \frac{1}{1+j\omega CR}V_{in1} + \frac{j\omega CR}{1+j\omega CR}V_{in2}$$

$$V_{out2} = -\frac{j\omega CR}{1+j\omega CR}V_{in1} + \frac{1}{1+j\omega CR}V_{in2}$$

In an alternative form:

$$V_{out1} = \frac{1}{1+j\omega/\omega_o}V_{in1} + \frac{j\omega/\omega_o}{1+s/\omega_o}V_{in2}$$

$$V_{out2} = -\frac{j\omega/\omega_o}{1+j\omega/\omega_o}V_{in1} + \frac{1}{1+j\omega/\omega_o}V_{in2}$$

$$\omega_o \equiv 1/RC$$

In matrix form:

$$\begin{bmatrix} V_{out1} \\ V_{out2} \end{bmatrix} = \begin{bmatrix} \dfrac{1}{1+j\omega/\omega_o} & \dfrac{j\omega/\omega_o}{1+j\omega/\omega_o} \\ -\dfrac{j\omega/\omega_o}{1+j\omega/\omega_o} & \dfrac{1}{1+j\omega/\omega_o} \end{bmatrix} \times \begin{bmatrix} V_{in1} \\ V_{in2} \end{bmatrix}$$

A positive sequence input in the time domain:

$$v_{in1}(t) = \cos(\omega t)$$
$$v_{in2}(t) = \sin(\omega t)$$

In the phasor domain:

$$V_{in1} = 1$$
$$V_{in2} = -j$$

These inputs result in:

$$V_{out1} = \frac{1+\omega/\omega_o}{1+j\omega/\omega_o} = 1 \times \frac{1+\omega/\omega_o}{1+j\omega/\omega_o}$$
$$V_{out2} = \frac{-j\omega/\omega_o - j}{1+j\omega/\omega_o} = -j \times \frac{1+\omega/\omega_o}{1+j\omega/\omega_o}$$

Therefore, the overall transfer function for a positive frequency input can be simplified to:

$$\begin{bmatrix} V_{out1} \\ V_{out2} \end{bmatrix} = \begin{bmatrix} \dfrac{1+\omega/\omega_o}{1+j\omega/\omega_o} & 0 \\ 0 & \dfrac{1+\omega/\omega_o}{1+j\omega/\omega_o} \end{bmatrix} \times \begin{bmatrix} V_{in1} \\ V_{in2} \end{bmatrix}$$

The magnitude for a positive sequence response simplifies to:

$$\left|H_{+\omega}\right| = \frac{\left|1+\omega/\omega_o\right|}{\sqrt{1+(\omega/\omega_o)^2}}$$

A negative sequence input in the time domain:

$$v_{in2}(t) = \sin(\omega t)$$
$$v_{in2}(t) = -\sin(\omega t)$$

In the phasor domain:

$$V_{in1} = 1$$

$$V_{in2} = j$$

These inputs result in:

$$\begin{aligned} V_{out1} &= \frac{1 - \omega/\omega_o}{1 + j\omega/\omega_o} &&= 1 \times \frac{1 - \omega/\omega_o}{1 + j\omega/\omega_o} \\ V_{out2} &= \frac{-j\omega/\omega_o + j}{1 + j\omega/\omega_o} &&= j \times \frac{1 - \omega/\omega_o}{1 + j\omega/\omega_o} \end{aligned}$$

Therefore, the overall transfer function for a positive frequency input simplifies to:

$$\begin{bmatrix} V_{out1} \\ V_{out2} \end{bmatrix} = \begin{bmatrix} \frac{1 - \omega/\omega_o}{1 + j\omega/\omega_o} & 0 \\ 0 & \frac{1 - \omega/\omega_o}{1 + j\omega/\omega_o} \end{bmatrix} \times \begin{bmatrix} V_{in1} \\ V_{in2} \end{bmatrix}$$

The magnitude response for negative frequency inputs can simplify to:

$$\left|H_{-\omega}\right| = \frac{\left|1 - \omega/\omega_o\right|}{\sqrt{1 + \left(\omega/\omega_o\right)^2}}$$

The positive and negative frequency magnitude responses can combine:

$$H(s) = \frac{s/j\omega_o + 1}{s/\omega_o + 1}$$

This first order response has a single complex zero at $-j\omega_o$.

Remember that a sinusoid signal pair can be written as a sum of positive and negative sequences:

$$\begin{aligned} v_{in1} &= \cos(\omega t) \\ v_{in2} &= 0 \end{aligned} \quad \longleftrightarrow \quad \begin{aligned} v_{in1} &= \frac{1}{2}\cos(\omega t) + \frac{1}{2}\cos(\omega t) \\ v_{in2} &= \frac{1}{2}\sin(\omega t) + \left(-\frac{1}{2}\sin(\omega t)\right) \end{aligned}$$

So the circuit response to an input set like this is:

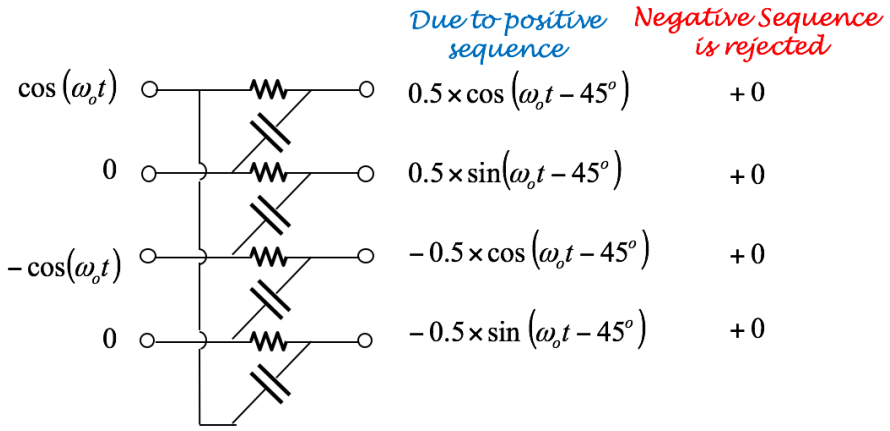

Because of how the circuit passes and blocks parts of the input signal, it has phase splitting properties. This means that the way multiple complex networks are cascaded affects their overall response.